In presenting the dissertation as a partial fulfillment of the requirements for an advanced degree from the Georgia Institute of Technology, I agree that the Library of the Institute shall make it available for inspection and circulation in accordance with its regulations governing materials of this type. I agree that permission to copy from, or to publish from, this dissertation may be granted by the professor under whose direction it was written, or, in his absence, by the Dean of the Graduate Division when such copying or publication is solely for scholarly purposes and does not involve potential financial gain. It is understood that any copying from, or publication of, this dissertation which involves potential financial gain will not be allowed without written permission.

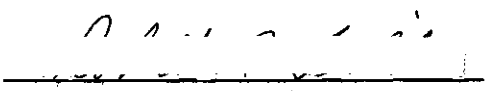

7/25/68

MEASUREMENT OF THIRD-ORDER ELASTIC CONSTANTS OF NACL USING LONGITUDINAL AND TRANSVERSE ULTRASONIC WAVES

A THESIS

Presented to

The Faculty of the Graduate Division

by

Robert Neil Trebits

In Partial Fulfillment

of the Requirements for the Degree

Doctor of Philosophy in the School of Physics

Georgia Institute of Technology

March, 1972

MEASUREMENT OF THIRD-ORDER ELASTIC CONSTANTS OF NACL USING LONGITUDINAL AND TRANSVERSE ULTRASONIC WAVES

Approved: _____

_____
Chairman

_____

_____

Date approved by Chairman: 2-22-72

ACKNOWLEDGMENTS

The author wishes to thank Dr. A. L. Stanford for not only the guidance and counsel given during the course of this work, but also the constructive criticism and encouragement which enabled the author to achieve a long sought, but often dimly seen, goal. Additional thanks are due to those on the reading committee, Dr. Joseph Ford and Dr. Stephen Spooner, for their many helpful comments.

The author also wishes to acknowledge the infinite faith of his parents, Mr. and Mrs. Max Trebits, in him. Finally, the author wishes to thank his loving wife P. J., without whose great patience and encouragement this work hardly would have been possible, and his adorable daughter Deidre, without whose presence this work might not have been necessary!

TABLE OF CONTENTS

TABLE OF CONTENTS (Concluded)

LIST OF TABLES

LIST OF ILLUSTRATIONS

LIST OF ILLUSTRATIONS (Concluded)

SUMMARY

The third-order elastic constants of a solid represent a measure of the anharmonic properties of that material. In particular these constants appear as coefficients in the theoretical expressions for quantities such as thermal expansion and ultrasonic wave attenuation. Heretofore, experimental measurements of third-order elastic constants have, for the most part, been made by determining the variation of acoustic wave velocity as a function of hydrostatic pressure or uniaxial stress. However, some recent determinations of the third-order elastic constants have utilized, in addition, measurements of second harmonic generation from initially sinusoidal, finite amplitude, longitudinal ultrasonic waves. The purpose of this research is to extend this second harmonic generation technique to include the use of transverse excitations, and to determine the full set of third-order elastic constants for single crystal sodium chloride.

Absolute displacement amplitudes were measured in three crystals at both the fundamental and second harmonic frequencies for longitudinal waves propagating in either the [100], [110], or [111] crystallographic direction. The actual displacement amplitudes were determined using the capacitance microphone technique, which is most suitable for this purpose. From these three samples one obtains numeric values for three linearly independent combinations of third-order elastic constants for sodium chloride.

Rather than obtain additional combinations of third-order elastic

constants by measuring longitudinal displacements in still other crystallographic directions, or resort to the usual hydrostatic pressure or uniaxial stress techniques, the technique of second harmonic generation was used again, but utilizing transverse acoustic waves. Since the capacitance microphone is incapable of measuring transverse displacements, a magnetic detection technique was perfected, which allowed displacement measurements for either longitudinal or transverse acoustic beams. The accuracy of this magnetic detection system was verified by repeating those measurements made using longitudinal vibrations propagating along the [100] and [111] directions.

Thus, two additional linear combinations of third-order elastic constants were obtained using this technique, one from waves polarized in the $[\bar{2}11]$ direction propagating along the [111] direction, and the other from waves polarized in the $[\bar{1}\bar{1}5]$ direction propagating along the [221] direction. The five linear combinations of elastic constants so obtained are the maximum number allowable when using the technique of second harmonic generation.

In order to determine values for the six distinct third-order elastic constants for a cubic structure such as sodium chloride, a sixth relationship among the elastic constants is required. Theoretical work has suggested that the Cauchy relation $C_{144} = C_{456}$ remains true even at elevated temperatures. With the assumption of this relationship, the six third-order elastic constants for sodium chloride were determined to have the values $C_{111} = -9.5$, $C_{112} = -0.79$, $C_{144} = +0.19$, $C_{166} = -0.83$, $C_{123} = +0.90$, and $C_{456} = +0.19$ in units of 10^{12} dynes/cm^2.

CHAPTER I

INTRODUCTION

Motivation

In 1676 Hooke (1) published the famous law which bears his name in the anagram ceiiinosssttuv. Reconstituted, these letters form the words ut tensio sic vis, that is, "The power of any spring is in the same proportion with the tension thereof." In contemporary language this statement takes the succinct form, "Stress is proportional to strain." However, this linear relationship fails to explain such well known phenomena as non-metallic thermal conductivity, thermal expansion (2), the temperature dependence of the second-order elastic constants (3), attenuation of ultrasonic waves in solids (4), and the interaction of acoustic and thermal phonons (5). The finite elastic theories of recent years endeavor to explain these deviations from the predictions of Hooke's law.

In the formalism of the microscopic theory of elasticity, the elastic potential energy density U of a crystal is expanded as a Taylor series about the equilibrium configuration of the lattice in the form

$$U = \frac{1}{2} \sum_{i,j,k,\ell=1}^{3} c_{ijk\ell}\, \xi_{ij}\xi_{k\ell} + \frac{1}{3!} \sum_{i,j,k,\ell,m,n=1}^{3} c_{ijk\ell mn}\, \xi_{ij}\xi_{k\ell}\xi_{mn} + \cdots, \tag{1}$$

where the ξ's are displacements from atomic equilibrium positions and

the c's are generally referred to as the microscopic coupling parameters. These coupling parameters are then just the spatial derivatives of the elastic potential energy density U, referred to the equilibrium positions. The zeroth-order term in this expansion is set equal to zero, and the first-order term vanishes, as the expansion is made about the equilibrium configuration. If one knew these microscopic coupling parameters, all the transport properties of the crystal could then be determined. Measuring these parameters requires the generation of acoustic waves with wavelengths comparable to the interatomic spacings. It is not experimentally possible at present, however, to generate ultrasonic waves having the requisite high frequencies.

For the wavelength range currently available, it is permissible to treat the solid as a continuum which has a constant mass density in the unstrained state. The elastic potential energy density U is then expanded in a Taylor series in the strain tensor elements in the form

$$U = \frac{1}{2} \sum_{i,j,k,\ell=1}^{3} C_{ijk\ell}\eta_{ij}\eta_{k\ell} + \frac{1}{3!} \sum_{i,j,k,\ell,m,n=1}^{3} C_{ijk\ell mn}\eta_{ij}\eta_{k\ell}\eta_{mn} + \cdots, \quad (2)$$

where the strain tensor elements η are defined in Equation (3) in Chapter II, and the C's are the elastic constants. As before, the zeroth-order term is set equal to zero, as this term represents the energy density of the solid at equilibrium, which is independent of the strain. Also, the first-order term vanishes if the underformed crystal state involves no external forces.

Obviously the elastic constants are not as fundamental as the microscopic coupling parameters, since the latter are directly derivable

from the interatomic potential energy of the crystal. However, using the various symmetry properties of a lattice structure, one can establish a relationship between the elastic constants and the microscopic coupling parameters. In particular, for the special case of nearest neighbor forces in a face-centered cubic lattice, Pfleiderer (6) and Coldwell-Horsfall (7) express the second- and third-order coupling parameters in terms of the second- and third-order elastic constants. Explicit relations of this type were also obtained by Coldwell-Horsfall (7) for body-centered cubic lattices using nearest and next-nearest neighbor interactions. Thus, in this rather indirect approach, one can determine information about the microscopic level (interatomic potential energy) by measuring macroscopic quantities (elastic constants).

If the elastic potential energy density is expressed in terms which are quadratic in the strain elements only, and linear elastic theory is used, a linear relationship between stress and strain results, Hooke's law. This procedure yields the so-called harmonic approximation and is quite sufficient to describe many of the physical properties of solids. To explain anharmonic effects, one must, at the least, retain third-order terms in the strain tensor elements in the expression for the elastic potential energy density. Thus, the determination of third-order elastic constants, to which end this work is directed, enables one to write down an explicit expression for the potential energy density function about an atomic site in a crystal structure. One can then hope to better understand those effects for which a simpler Hookean explanation is insufficient.

Historical Background

Cauchy (8) had by 1822 formulated much of the linear theory of elasticity. A non-linear theory was established in tensor notation by Brillouin (9) in 1925. Murnaghan (10) reformulated the theory in the matrix notation, which will be used here. Murnaghan's theory of finite strains was developed by Birch (11) for media of cubic symmetry, including terms to third order in the strain elements in the elastic potential energy density. Hearmon (12, 13) summarized previous work in the area and enumerated the distinct, independent second- and third-order elastic constants for all crystal classes. Brugger (14) presented general thermodynamic definitions for the higher order elastic constants in 1964 in tensor and in engineering notation. Because Brugger's notation will be adopted here, the relationships between this notation and that of Birch is indicated in Table 1.

In recent years much work has been done in theoretical calculations of the elastic constants for various materials. Ghate (15) has estimated the third-order elastic constants for NaCl-type and CsCl-type crystals using the Born model of ionic solids. Short-range interactions were included up to next-nearest neighbors. The linear temperature dependence of the elastic constants was also determined, in the high-temperature limit. Lincoln, Koliwad, and Ghate (16) calculated the second- and third-order elastic constants for Al, Cu, Ag, Au, Na, and K from a central-force model which was based on an interatomic potential function expressed in terms of the Morse potential. The electrostatic and repulsive ion-ion contributions to the elastic constants were deduced by Cousins (17) for face-centered and body-centered cubic structure

metals. In 1970 Suzuki (18) calculated the elastic constants for Al and Pb from derivatives of the binding energy function derived from a local pseudo-potential.

There has also been no shortage of experimenters and experiments to determine the magnitudes of elastic constants of different materials. One generally categorizes these methods as hydrostatic pressure, uni-axial stress, acoustic-optic, acoustic mixing, or second harmonic generation techniques. It will be instructive to briefly review some of the work done in recent years using each of these techniques for determining elastic constants.

From the equations of motion describing an elastic medium, one can relate the second-order elastic constants with the velocities of acoustic waves propagating in various crystallographic directions through the solid. If one includes anharmonic terms in the equation of motion, the wave velocity is found to depend also on the third-order elastic constants. In a pioneer experiment performed in 1949 Lazarus (19) made such velocity measurements as a function of hydrostatic presure on crystals of KCl, NaCl, CuZn, Cu, and Al. In 1958 Daniels and Smith (20) measured the pressure derivatives of the elastic constants of the homologous series of metals Cu, Ag, and Au. In 1962 McSkimin and Andreatch (21) investigated the acoustic wave velocities of high purity germanium as a function of both pressure and temperature. Chang and Barsch (22) in 1967 measured the pressure dependence of the elastic constants of the cesium halides and determined three linear combinations of fourth-order elastic constants for this group. This experimental technique lends itself to materials which might undergo plastic strain

under relatively small stresses. Unfortunately measurements using hydrostatic pressure variations do not allow one to determine a complete set of third-order elastic constants.

One can, however, obtain the entire set of desired constants by combining the results of hydrostatic pressure experiments with those obtained by using the technique of change in acoustic wave velocity in a crystal with applied uniaxial stress. Hughes and Kelly (23) measured the transmission times of elastic pulses traveling through such isotropic materials as polystyrene, iron, and Pyrex glass under uniaxial stress. Bateman, Mason, and McSkimin (24) in 1960 were able, for the first time, to determine the six third-order elastic constants of a cubic material, germanium, using this technique. McSkimin and Andreatch (25) in 1964 extended the number of complete sets of constants with their measurements on silicon, and improved upon the accuracy of the data on germanium. The third-order elastic constants of germanium, magnesium oxide, and fused silica were found in 1965 by Bogardus (26) using a pulse superposition detection apparatus to determine the ultrasonic velocity as a function of both uniaxial stress and hydrostatic pressure. Thurston, McSkimin, and Andreatch (27) found all fourteen of the third-order elastic constants of quartz in 1965. Chang (28) combined uniaxial stress measurements for NaCl and KCl single crystals with Lazarus' data to determine the elastic constants for these materials. The same year Hiki and Granato (29) found values for the third-order elastic constants of high purity copper, silver, and gold single crystals at room temperature and estimated the fourth-order constants. In 1968 Thomas (30) used an interferometric technique to find the third-order constants of aluminum

single crystals. Powell and Skove (31) measured the elastic constants of whiskers of copper, silver, and iron and fibers of fused quartz in 1968 and estimated the fourth-order constants for this form of quartz.

Since the use of either hydrostatic pressure or uniaxial stress techniques involves the possibility of plastic deformation to the crystal under measurement, it is of considerable interest to determine the values of elastic constants by less potentially destructive methods. One such procedure utilizes the diffraction pattern produced by a monochromatic light beam passing through a transparent sample perpendicular to an initially sinusoidal ultrasonic wave propagating through the material, as suggested by Melngailis, Maradudin, and Seeger (32) in 1963. The asymmetry in the intensity of the diffraction pattern can then be related to the third-order elastic constants of the crystal. Measurement of one of the third-order elastic constants of NaCl was carried out in this manner in 1964 by Parker, Kelly, and Bolef (33).

Yet a different approach to the problem utilizes the interaction of two intersecting ultrasonic beams in a crystal, which generates a scattered wave. Knowing the amplitudes of both input and scattered waves and the geometric parameters of the experiment, one can measure a value for linear combinations of third-order elastic constants of the crystal. Such phonon-phonon experiments were made by Rollins (34) in 1963 and by Rollins, Taylor, and Todd (35) in 1964. A quantum mechanical calculation of the phonon-phonon interaction was made in 1964 by Taylor and Rollins (36) and its application to the determination of third-order elastic constants by Childress and Hambrick (37). In 1961 Carr (38) used harmonic generation of microwave phonons by wave interaction to

measure the elastic constants of MgO. Holt (39) in 1967 tabulated a set of phonon-phonon interactions for cubic materials which could be useful for measuring elastic constants. Experimental determinations of combinations of third-order elastic constants for fused silica and for single crystal NaCl were recently made in 1970 by Dunham and Huntington (40).

The technique of harmonic generation as a means for determining elastic constants has its roots in the observations of Mendousse (41) in 1952, Gedroits and Krasil'nikov (42) in 1962, and Blackstock (43) in 1965. It was noted that originally sinusoidal acoustic waves propagating in a nonlinear solid became distorted, and that the amount of second harmonic thus produced could be related to the elastic constants of the material. The amplitude of the second harmonic generated is proportional to the square of the amplitude of the fundamental, to the distance traveled in the solid, and to a non-linearity factor which is a combination of second- and third-order elastic constants. If one assumes that the second-order constants are known, the third-order constants can then be determined by measuring the absolute amplitudes of both the fundamental and second harmonic acoustic waves. Breazeale and Ford (44) showed that longitudinal waves propagating in the [100], [110], or [111] direction yield three linearly independent combinations of third-order elastic constants. In 1966 Buck and Thompson (45) found those constants and combinations of constants which, in principle, could be obtained using this technique. Holt and Ford (46) in 1966 calculated those combinations of third-order elastic constants which could be obtained using acoustic waves of specified polarization and propagation directions

in cubic materials. They noted that harmonic generation does not yield all six third-order elastic constants for cubic materials, and that the results of such experiments would have to be combined with data obtained using some other technique to achieve such a set.

An experimental determination of third-order elastic constants using harmonic generation was made by Gedroits and Krasil'nikov (42) in 1962 for Al, NaCl, KCl, and LiF; by Breazeale and Thompson (47) in 1963 for aluminum; and by Gauster and Breazeale (48) in 1966 for copper single crystals. These last investigators used as an acoustic detector a capacitance microphone developed by Peters, Breazeale, and Paré (49). Hikata, Chick, and Elbaum (50) in 1965 measured a dislocation contribution to the second harmonic generation of ultrasonic waves in aluminum single crystals. Third harmonic generation has been used by Peters and Arnold (51) in the determination of the temperature dependence of one of the third-order elastic constants of $SrTiO_3$ single crystals.

The Elastic Constants of Sodium Chloride

Because of a relatively simple lattice structure, sodium chloride has been a favorite material of those who have calculated the third-order elastic constants from first principles. Nran'yan (52) calculated the constants for NaCl-type structures using the Born model with nearest neighbor interactions, while Ghate (15) used the Born-Mayer potential for short-range repulsive interactions and included next-nearest neighbor effects. In 1969 Paul (53, 54) investigated the effect of the three-body interaction on the third-order elastic constants of the alkali halides, and included in the total potential

function the Coulomb interaction, the overlap interaction in exponential form, and the van der Waals interaction.

All the measurement techniques described have been utilized to some extent in the determination of the third-order elastic constants of sodium chloride. Swartz (55) in 1966 used uniaxial stress data with the results of hydrostatic pressure experiments to find a complete set of six constants. Ghafelehbashi and Koliwad (56) in 1970 used hydrostatic pressure to measure the pressure derivatives of the second-order elastic constants. Uniaxial stress methods have been used extensively by Chang (28) in 1965, by Drabble and Strathen (57) in 1967, and by Gluyas (58) the same year, all on sodium chloride. Parker, Kelly, and Bolef (33) used the newly developed acoustic-optic technique to calculate one of the third-order elastic constants of NaCl, while Dunham and Huntington (40) used the phonon-phonon interaction method.

Harmonic generation methods were used by Stanford and Zehner (59) in 1966 to determine one of the third-order elastic constants for both NaCl and KCl. Mikhailov and Shutilov (60) in 1963 suggested that a magnetic-electric method of acoustic wave detection could be useful in determining ultrasonic properties of solids. The innovation of both of these approaches to the problem of determining a complete set of third-order elastic constants provided the impetus for the present work. Using both the capacitance microphone and magnetic detector techniques, we here obtain five linear combinations of the six sought constants for sodium chloride. With the acceptance of the validity of a sixth, theoretical, relationship among the constants, the full set of third-order elastic constants for sodium chloride will be calculated.

CHAPTER II

THEORY OF HARMONIC GENERATION

The velocities of ultrasonic pulses in sodium chloride are on the order of 5×10^3 m/sec. Since the frequency of fundamental operation in this experiment was 30 MHz, the corresponding wavelength was about 1.7×10^{-4} meters. The lattice parameter a for sodium chloride is 5.63 Å. For this crystal structure, the nearest neighbor distance for like atoms is $a/\sqrt{2}$, or about 4 Å. Thus, one wavelength of the ultrasonic signal is some 100,000 times longer than the lattice spacings of the crystal, and it will be quite justifiable to regard the solid as an elastic continuum. Since large amplitude displacements are involved, Murnaghan's finite deformation elastic theory (10) will be used to develop the equations of motion for a point in a medium of cubic symmetry.

The Strain Tensor

Let a point in the continuum of the medium have the Cartesian coordinates (a_1, a_2, a_3) in the initial, or unstrained, state. The Cartesian coordinates of the same point at some later time in a strained, or deformed, state are given by (x_1, x_2, x_3). Then the Lagrangian strain tensor for finite deformations is defined by the relation

$$\eta_{ij} = \frac{1}{2}\left[\sum_{k=1}^{3} \frac{\partial x_k}{\partial a_i}\,\frac{\partial x_k}{\partial a_j} - \delta_{ij}\right], \tag{3}$$

where δ_{ij} is the Kroneker δ, and the subscripts i and j take on the

values 1,2,3. It is seen by inspection that the strain tensor is symmetric. One also notes that the origin of the initial, unstrained reference frame need not coincide with the origin of the final, deformed frame.

The strain matrix may be expressed in terms of the Jacobian matrix J of the transformation from the initial to final coordinate systems:

$$J = \frac{\partial(x_1,x_2,x_3)}{\partial(a_1,a_2,a_3)} = \begin{pmatrix} \frac{\partial x_1}{\partial a_1} & \frac{\partial x_1}{\partial a_2} & \frac{\partial x_1}{\partial a_3} \\ \frac{\partial x_2}{\partial a_1} & \frac{\partial x_2}{\partial a_2} & \frac{\partial x_2}{\partial a_3} \\ \frac{\partial x_3}{\partial a_1} & \frac{\partial x_3}{\partial a_2} & \frac{\partial x_3}{\partial a_3} \end{pmatrix}. \qquad (4)$$

The final coordinates (x_1, x_2, x_3) are assumed to be differentiable functions of (a_1, a_2, a_3), and the determinant of the Jacobian matrix, $\det \frac{\partial(x_1,x_2,x_3)}{\partial(a_1,a_2,a_3)}$, is assumed to be positive. Then the volume element dV_x of the final state is given by the expression

$$dV_x = dx_1dx_2dx_3 = \det \frac{\partial(x_1,x_2,x_3)}{\partial(a_1,a_2,a_3)}\, da_1da_2da_3 = (\det J)\, dV_a. \qquad (5)$$

For a rigid displacement, i.e., no deformation, or a pure rotation, J^*J is the unit matrix I, where J^* is the transpose of J. To eliminate either of these cases, we can write the strain matrix as the difference

between J^*J and I as a measure of the deformation of the medium about a point (a_1, a_2, a_3):

$$[\eta] = \frac{1}{2}[J^*J - I] , \tag{6}$$

where the factor of $\frac{1}{2}$ is necessary to insure agreement with infinitesimal theory. Equation (6) yields the same strain elements η_{ij} as does Equation (3).

Generalized Definition of the Elastic Constants

The elastic potential energy density U of a solid can be expanded in terms of powers of the strain components. We express U as a sum of terms, where each term contains the strain elements to the power indicated by the term subscript. Thus we have the relation

$$U = U_0 + U_1 + U_2 + U_3 + \cdots . \tag{7}$$

U_0 is just the free energy of a solid in equilibrium and may be set equal to zero, since U_0 is strain-independent. U_1 is also zero, as the initial state is the undeformed equilibrium state. All terms higher than third order in the strain elements are assumed to be negligibly small, justified by experimental considerations.

The remaining terms in Equation (7), U_2 and U_3, are given by

$$U_2 = \frac{1}{2!} \sum_{\substack{ijk\ell \\ =1}}^{3} C_{ijk\ell}\eta_{ij}\eta_{k\ell} \tag{8}$$

and

$$U_3 = \frac{1}{3!} \sum_{\substack{ijk\ell mn \\ =1}}^{3} C_{ijk\ell mn} \eta_{ij} \eta_{k\ell} \eta_{mn} , \qquad (9)$$

where all subscripts take on the value 1, 2, 3. Thus, including terms cubic in the strain elements in Equation (7) goes one term beyond the approximation of Hooke's law. The $C_{ijk\ell}$ and $C_{ijk\ell mn}$ in Equations (8) and (9) are the second- and third-order elastic constants respectively in tensor notation. Considering all possible combinations of the subscripts of the elastic constants, there are some 81 possible second-order and 729 possible third-order elastic constants. However, Birch has shown that one can greatly reduce the number of independent constants by considering the symmetry properties of the crystal. For the class of cubic crystals, there are but three distinct, non-zero, second-order elastic constants. If we also restrict ourselves to those cubic crystals, such as NaCl, with the very highest order of symmetry, the number of distinct, non-zero, third-order elastic constants is reduced to six.

Thus, for the special case of sodium chloride, we may write the elastic potential energy density, using Brugger's notation, as

$$\begin{aligned} U(\eta) = {} & \frac{1}{2} C_{11}[\eta_{11}^2 + \eta_{22}^2 + \eta_{33}^2] + C_{12}[\eta_{11}\eta_{22} + \eta_{22}\eta_{33} + \eta_{33}\eta_{11}] \qquad (10) \\ & + 2C_{44}[\eta_{12}^2 + \eta_{31}^2 + \eta_{23}^2] + \frac{1}{6} C_{111}[\eta_{11}^3 + \eta_{22}^3 + \eta_{33}^3] \\ & + \frac{1}{2} C_{112}[(\eta_{22} + \eta_{33})\eta_{11}^2 + (\eta_{11} + \eta_{22})\eta_{33}^2 + (\eta_{11} + \eta_{33})\eta_{22}^2] \\ & + C_{123}[\eta_{11}\eta_{22}\eta_{33}] + 2C_{144}[\eta_{11}\eta_{23}^2 + \eta_{22}\eta_{31}^2 + \eta_{33}\eta_{12}^2] \end{aligned}$$

$$+ 2c_{166}[(\eta_{11} + \eta_{22})\eta_{12}^2 + (\eta_{22} + \eta_{33})\eta_{23}^2 + (\eta_{11} + \eta_{33})\eta_{13}^2] + 8c_{456}\eta_{12}\eta_{23}\eta_{31},$$

where the strain elements η_{ij} are calculated using coordinate axes parallel to the crystal symmetry axes. In Equation (10) we have utilized the conventional contraction of subscripts of the tensor elastic constants:

$11 \rightarrow 1$	$33 \rightarrow 3$	$31 \rightarrow 5$
$22 \rightarrow 2$	$23 \rightarrow 4$	$12 \rightarrow 6$

Equation (10) differs from Birch's expression for the elastic potential energy density by various constant factors, since Brugger's notation for the elastic constants is not the same as that of Birch. Table 1 lists a comparison of Brugger's notation with that used by Birch.

The Equations of Motion

One can derive the equations of motion directly from the expression for the elastic potential energy density and from Lagrange's equations for continuous media. If we let ρ be the mass density of the medium in its initial unstrained state, then the Lagrangian density for the system is

$$\mathcal{L} = \frac{1}{2}\sum_{i=1}^{3}\rho\dot{x}_i^2 - U(\eta), \tag{11}$$

where the dot denotes differentiation with respect to time.

Lagrange's equations for continuous media are

Table 1. Comparison of Birch's Notation for Third-order Elastic Constants with that of Brugger's Used Here

Brugger's (present) Notation	Birch's Notation
C_{111}	$6\,C^{B}_{111}$
C_{112}	$2\,C^{B}_{112}$
C_{123}	C^{B}_{123}
C_{144}	$\frac{1}{2}\,C^{B}_{144}$
C_{166}	$\frac{1}{2}\,C^{B}_{166}$
C_{456}	$\frac{1}{4}\,C^{B}_{456}$

$$\frac{d}{dt}\left[\frac{\partial \mathcal{L}}{\partial \dot{x}_i}\right] + \sum_{k=1}^{3} \frac{d}{da_k}\left[\frac{\partial \mathcal{L}}{\partial\left(\frac{\partial x_i}{\partial a_k}\right)}\right] = 0 , \tag{12}$$

where i takes on the values 1, 2, 3. Combining Equations (11) and (12), one obtains

$$\rho \ddot{x}_i - \sum_{j,k,\ell=1}^{3} \frac{d}{da_j}\left[\frac{\partial U}{\partial \eta_{k\ell}} \frac{\partial \eta_{k\ell}}{\partial\left(\frac{\partial x_i}{\partial a_j}\right)}\right] = 0. \tag{13}$$

Differentiation of Equation (3) with respect to $\frac{\partial x_i}{\partial a_j}$ yields

$$\frac{\partial \eta_{k\ell}}{\partial\left(\frac{\partial x_i}{\partial a_j}\right)} = \frac{1}{2}\,\delta_{jk}\frac{\partial x_i}{\partial a_\ell} + \frac{1}{2}\,\delta_{j\ell}\frac{\partial x_i}{\partial a_k} . \tag{14}$$

If we use the Jacobian notation for Equation (4)

$$J_{ij} = \frac{\partial x_i}{\partial a_j} , \tag{15}$$

then Equation (14) can be written in the form

$$\frac{\partial \eta_{k\ell}}{\partial\left(\frac{\partial x_i}{\partial a_j}\right)} = \frac{1}{2}\,\delta_{jk}\,J_{i\ell} + \frac{1}{2}\,\delta_{j\ell}J_{ik} . \tag{16}$$

With the substitution of Equation (16) into Equation (13), one obtains the equations of motion of the system in the usual form:

$$\rho \ddot{x}_i = \sum_{k,\ell=1}^{3} \frac{d}{da_k}\left[J_{i\ell}\frac{\partial U}{\partial \eta_{k\ell}}\right] , \tag{17}$$

where it has been assumed that $U(\eta)$ is of the form such that

$$\frac{\partial U}{\partial \eta_{k\ell}} = \frac{\partial U}{\partial \eta_{\ell k}} \quad . \tag{18}$$

If we define the particle displacement vector u_i to be

$$u_i = x_i - a_i \quad , \tag{19}$$

then Equation (15) can be written as

$$J_{i\ell} = \frac{\partial x_i}{\partial a_\ell} = \frac{\partial u_i}{\partial a_\ell} + \delta_{i\ell} \quad , \tag{20}$$

and the equations of motion become

$$\rho \ddot{u}_i = \sum_{k,\ell=1}^{3} \frac{d}{da_k}\left[\frac{\partial u_i}{\partial a_\ell} \frac{\partial U}{\partial \eta_{\ell k}} + \frac{\partial U}{\partial \eta_{ik}} \right]. \tag{21}$$

One takes the appropriate derivatives of the elastic potential energy density U with respect to η, and expresses the results in terms of $\frac{\partial u}{\partial a}$. The terms are then collected, and products of three or more derivatives are dropped. Three coupled partial differential equations are obtained, one for each of the particle displacements u_i, with the a_i and t as independent variables. The first of these equations is

$$\rho \ddot{u}_1 = C_{11} \frac{\partial^2 u_1}{\partial a_1^2} + C_{12} \left(\frac{\partial^2 u_2}{\partial a_1 \partial a_2} + \frac{\partial^2 u_3}{\partial a_1 \partial a_3} \right) + C_{44} \left(\frac{\partial^2 u_1}{\partial a_2^2} + \frac{\partial^2 u_1}{\partial a_3^2} + \frac{\partial^2 u_2}{\partial a_1 \partial a_2} + \frac{\partial^2 u_3}{\partial a_1 \partial a_3} \right) \tag{22}$$

$$+ C_{11}\Big[3\,\frac{\partial u_1}{\partial a_1}\,\frac{\partial^2 u_1}{\partial a_1^2} + \frac{\partial u_2}{\partial a_2}\,\frac{\partial^2 u_1}{\partial a_2^2} + \frac{\partial u_3}{\partial a_3}\,\frac{\partial^2 u_1}{\partial a_3^2} + \frac{\partial u_2}{\partial a_1}\,\frac{\partial^2 u_2}{\partial a_1^2} + \frac{\partial u_1}{\partial a_2}\,\frac{\partial^2 u_2}{\partial a_2^2}$$

$$+ \frac{\partial u_3}{\partial a_1}\,\frac{\partial^2 u_3}{\partial a_1^2} + \frac{\partial u_1}{\partial a_3}\,\frac{\partial^2 u_3}{\partial a_3^2}\Big]$$

$$+ C_{12}\Big[\Big(\frac{\partial u_2}{\partial a_2} + \frac{\partial u_3}{\partial a_3}\Big)\,\frac{\partial^2 u_1}{\partial a_1^2} + \Big(\frac{\partial u_1}{\partial a_1} + \frac{\partial u_3}{\partial a_3}\Big)\,\frac{\partial^2 u_1}{\partial a_2^2} + \Big(\frac{\partial u_1}{\partial a_1} + \frac{\partial u_2}{\partial a_2}\Big)\,\frac{\partial^2 u_1}{\partial a_3^2}$$

$$+ 2\,\frac{\partial u_1}{\partial a_2}\,\frac{\partial^2 u_1}{\partial a_1 \partial a_2} + 2\,\frac{\partial u_1}{\partial a_3}\,\frac{\partial^2 u_1}{\partial a_1 \partial a_3} + \Big(\frac{\partial u_1}{\partial a_1} + \frac{\partial u_2}{\partial a_2}\Big)\,\frac{\partial^2 u_2}{\partial a_1 \partial a_2}$$

$$+ \frac{\partial u_2}{\partial a_3}\,\frac{\partial^2 u_2}{\partial a_1 \partial a_3} + \frac{\partial u_1}{\partial a_3}\,\frac{\partial^2 u_2}{\partial a_2 \partial a_3} + \frac{\partial u_3}{\partial a_2}\,\frac{\partial^2 u_3}{\partial a_1 \partial a_2} + \Big(\frac{\partial u_1}{\partial a_1} + \frac{\partial u_3}{\partial a_3}\Big)\,\frac{\partial^2 u_3}{\partial a_1 \partial a_3}$$

$$+ \frac{\partial u_1}{\partial a_2}\,\frac{\partial^2 u_3}{\partial a_2 \partial a_3}\Big]$$

$$+ C_{44}\Big[2\,\frac{\partial u_1}{\partial a_1}\,\Big(\frac{\partial^2 u_1}{\partial a_2^2} + \frac{\partial^2 u_1}{\partial a_3^2}\Big) + 2\Big(2\,\frac{\partial u_1}{\partial a_2} + \frac{\partial u_2}{\partial a_1}\Big)\,\frac{\partial^2 u_1}{\partial a_1 \partial a_2}$$

$$+ 2\,\Big(2\,\frac{\partial u_1}{\partial a_3} + \frac{\partial u_3}{\partial a_1}\Big)\,\frac{\partial^2 u_1}{\partial a_1 \partial a_3} + 2\,\Big(\frac{\partial u_2}{\partial a_3} + \frac{\partial u_3}{\partial a_2}\Big)\,\frac{\partial^2 u_1}{\partial a_2 \partial a_3} + \frac{\partial u_1}{\partial a_2}\,\frac{\partial^2 u_2}{\partial a_1^2}$$

$$+ \frac{\partial u_2}{\partial a_1}\,\frac{\partial^2 u_2}{\partial a_2^2} + \Big(\frac{\partial u_2}{\partial a_1} + \frac{\partial u_1}{\partial a_2}\Big)\,\frac{\partial^2 u_2}{\partial a_3^2} + \Big(\frac{\partial u_1}{\partial a_1} + \frac{\partial u_2}{\partial a_2}\Big)\,\frac{\partial^2 u_2}{\partial a_1 \partial a_2}$$

$$+ \frac{\partial u_2}{\partial a_3}\,\frac{\partial^2 u_2}{\partial a_1 \partial a_3} + \frac{\partial u_1}{\partial a_3}\,\frac{\partial^2 u_2}{\partial a_2 \partial a_3} + \frac{\partial u_1}{\partial a_3}\,\frac{\partial^2 u_3}{\partial a_1^2} + \Big(\frac{\partial u_1}{\partial a_3} + \frac{\partial u_3}{\partial a_1}\Big)\,\frac{\partial^2 u_3}{\partial a_2^2}$$

$$+ \frac{\partial u_3}{\partial a_1}\frac{\partial^2 u_3}{\partial a_3^2} + \frac{\partial u_3}{\partial a_2}\frac{\partial^2 u_3}{\partial a_1 \partial a_2} + \left(\frac{\partial u_1}{\partial a_1} + \frac{\partial u_3}{\partial a_3}\right)\frac{\partial^2 u_3}{\partial a_1 \partial a_3} + \frac{\partial u_1}{\partial a_2}\frac{\partial^2 u_3}{\partial a_2 \partial a_3}\Big]$$

$$+ C_{111}\frac{\partial u_1}{\partial a_1}\frac{\partial^2 u_1}{\partial a_1^2}$$

$$+ C_{112}\Big[\left(\frac{\partial u_2}{\partial a_2} + \frac{\partial u_3}{\partial a_3}\right)\frac{\partial^2 u_1}{\partial a_1^2} + \left(\frac{\partial u_1}{\partial a_1} + \frac{\partial u_2}{\partial a_2}\right)\frac{\partial^2 u_2}{\partial a_1 \partial a_2} + \left(\frac{\partial u_1}{\partial a_1} + \frac{\partial u_3}{\partial a_3}\right)\frac{\partial^2 u_3}{\partial a_1 \partial a_3}$$

$$+ C_{144}\Big[\frac{\partial u_3}{\partial a_3}\frac{\partial^2 u_1}{\partial a_2^2} + \frac{\partial u_2}{\partial a_2}\frac{\partial^2 u_1}{\partial a_3^2} + \frac{\partial u_3}{\partial a_3}\frac{\partial^2 u_2}{\partial a_1 \partial a_2} + \left(\frac{\partial u_3}{\partial a_2} + \frac{\partial u_2}{\partial a_3}\right)\frac{\partial^2 u_2}{\partial a_1 \partial a_3}$$

$$+ \left(\frac{\partial u_1}{\partial a_3} + \frac{\partial u_3}{\partial a_1}\right)\frac{\partial^2 u_2}{\partial a_2 \partial a_3} + \left(\frac{\partial u_2}{\partial a_3} + \frac{\partial u_3}{\partial a_2}\right)\frac{\partial^2 u_3}{\partial a_1 \partial a_2} + \frac{\partial u_2}{\partial a_2}\frac{\partial^2 u_3}{\partial a_1 \partial a_3}$$

$$+ \left(\frac{\partial u_1}{\partial a_2} + \frac{\partial u_2}{\partial a_1}\right)\frac{\partial^2 u_3}{\partial a_2 \partial a_3}\Big]$$

$$+ C_{166}\Big[\left(\frac{\partial u_1}{\partial a_1} + \frac{\partial u_2}{\partial a_2}\right)\frac{\partial^2 u_1}{\partial a_2^2} + \left(\frac{\partial u_1}{\partial a_1} + \frac{\partial u_3}{\partial a_3}\right)\frac{\partial^2 u_1}{\partial a_3^2} + 2\left(\frac{\partial u_1}{\partial a_2} + \frac{\partial u_2}{\partial a_1}\right)\frac{\partial^2 u_1}{\partial a_1 \partial a_2}$$

$$+ 2\left(\frac{\partial u_1}{\partial a_3} + \frac{\partial u_3}{\partial a_1}\right)\frac{\partial^2 u_1}{\partial a_1 \partial a_3} + \left(\frac{\partial u_1}{\partial a_2} + \frac{\partial u_2}{\partial a_1}\right)\left(\frac{\partial^2 u_2}{\partial a_1^2} + \frac{\partial^2 u_2}{\partial a_2^2}\right)$$

$$+ \left(\frac{\partial u_1}{\partial a_1} + \frac{\partial u_2}{\partial a_2}\right)\frac{\partial^2 u_2}{\partial a_1 \partial a_2} + \left(\frac{\partial u_1}{\partial a_3} + \frac{\partial u_3}{\partial a_1}\right)\left(\frac{\partial^2 u_3}{\partial a_1^2} + \frac{\partial^2 u_3}{\partial a_3^2}\right)$$

$$+ \left(\frac{\partial u_1}{\partial a_1} + \frac{\partial u_3}{\partial a_3}\right)\frac{\partial^2 u_3}{\partial a_1 \partial a_3}\Big]$$

$$+ C_{123} \left(\frac{\partial u_3}{\partial a_3} \frac{\partial^2 u_2}{\partial a_1 \partial a_2} + \frac{\partial u_2}{\partial a_2} \frac{\partial^2 u_3}{\partial a_1 \partial a_3}\right)$$

$$+ C_{456}\Bigg[2 \left(\frac{\partial u_2}{\partial a_3} + \frac{\partial u_3}{\partial a_2}\right) \frac{\partial^2 u_1}{\partial a_2 \partial a_3} + \left(\frac{\partial u_1}{\partial a_2} + \frac{\partial u_2}{\partial a_1}\right) \frac{\partial^2 u_2}{\partial a_3^2} + \left(\frac{\partial u_2}{\partial a_3} + \frac{\partial u_3}{\partial a_2}\right) \frac{\partial^2 u_3}{\partial a_1 \partial a_2}$$

$$+ \left(\frac{\partial u_2}{\partial a_3} + \frac{\partial u_3}{\partial a_2}\right) \frac{\partial^2 u_2}{\partial a_1 \partial a_3} + \left(\frac{\partial u_1}{\partial a_3} + \frac{\partial u_3}{\partial a_1}\right) \left(\frac{\partial^2 u_2}{\partial a_2 \partial a_3} + \frac{\partial^2 u_3}{\partial a_2^2}\right)$$

$$+ \left(\frac{\partial u_1}{\partial a_2} + \frac{\partial u_2}{\partial a_1}\right) \frac{\partial^2 u_3}{\partial a_2 \partial a_3}\Bigg] .$$

The corresponding equations for u_2 and u_3 can be obtained by cyclic permutation of the subscripts in Equation (22).

Nonetheless, Equation (22), which approximates Equation (21) by the omission of higher order terms, is still too complex and unwieldy to be very useful. The selection of particular propagation and polarization directions, however, further simplifies the problem. The number of equations can then be reduced to one, and the number of independent variables reduced from four to two, the time t and the distance a along the propagation direction.

Consider the simplest case: a plane, longitudinal acoustic wave propagating along the [100] crystallographic direction. The particle displacement u_1 thus depends only on t and a_1, where the a_1-axis is now in the propagation direction. Dropping the subscripts, Equation (22) here becomes

$$\rho \ddot{u} = C_{11} \frac{\partial^2 u}{\partial a^2} + \left[3C_{11} + C_{111}\right] \frac{\partial u}{\partial a} \frac{\partial^2 u}{\partial a^2} . \qquad (23)$$

To treat the case of plane waves propagating in directions other than the [100] direction, it proves advantageous to rotate the initial coordinate frame so that the new a_1-axis coincides with the propagation direction. Let us now recall that the elastic constants were defined in Equation (10) as the coefficients of the terms in the expansion of the elastic potential energy density U in powers of the strain elements, where the strain was calculated with the a_i-axes parallel to the symmetry axes of the crystal. Thus, we must determine the changes in the $U(\eta)$ and η of Equation (10) under a rotation of the a_i-axes in order that Equation (17) contain the conventionally defined elastic constants.

Consider a real rotation of the a_i-axes given by the matrix equation

$$a = R\bar{a} , \tag{24}$$

where R is a 3 x 3 orthogonal matrix which rotates the $\bar{a}_i$-axes into the a_i-axes. The bar superscript denotes a quantity calculated with the crystal axes parallel to the coordinate axes. Quantities without the bar are calculated with the a_i-axis parallel to the propagation direction. Murnaghan (10) has shown that the strain transforms as

$$\bar{\eta} = R^* \eta R , \tag{25}$$

where R^* is the transpose of R. Since the elastic potential energy density transforms as a scalar under a rotation, we must have

$$U(\eta) = U(\bar{\eta}) = U(R^{*}\eta R). \tag{26}$$

Equation (10) then becomes

$$U(\bar{\eta}) = \frac{1}{2} C_{11}(\bar{\eta})^2 + \cdots + \frac{1}{6} C_{111}(\bar{\eta})^3 + \cdots. \tag{27}$$

Putting the expression for $\bar{\eta}$ from Equation (25) into Equation (27) yields

$$U = \frac{1}{2} C_{11}\Big[\sum_{\substack{jk\\=1}}^{3} R^{*}_{1j}\eta_{jk}R_{k1}\Big]^2 + \cdots + \frac{1}{6} C_{111}\Big[\sum_{\substack{jk\\=1}}^{3} R^{*}_{1j}\eta_{jk}R_{k1}\Big] + \cdots. \tag{28}$$

Thus, the equations of motion become

$$\rho\ddot{u} = \frac{d}{da}\Big[\sum_{k=1}^{3} J_{ik}\frac{\partial U(R^{*}\eta R)}{\partial \eta}\Big]. \tag{29}$$

As an example, consider the case of longitudinal waves propagating in the [110] crystallographic direction. The initial coordinate frame is rotated by 45° about the a_3-axis so that the new a_1-axis coincides with the [110] direction in the crystal. The required rotation matrix is given by

$$R = \begin{pmatrix} \frac{1}{\sqrt{2}} & \frac{1}{\sqrt{2}} & 0 \\ -\frac{1}{\sqrt{2}} & \frac{1}{\sqrt{2}} & 0 \\ 0 & 0 & 1 \end{pmatrix}, \tag{30}$$

and the strain elements are related by the expression

$$\bar{\eta} = \begin{pmatrix} \frac{1}{2}(\eta_{11}-\eta_{12}-\eta_{21}+\eta_{22}) & \frac{1}{2}(\eta_{11}+\eta_{12}-\eta_{21}-\eta_{22}) & \frac{1}{\sqrt{2}}(\eta_{13}-\eta_{23}) \\ \frac{1}{2}(\eta_{11}-\eta_{12}+\eta_{21}-\eta_{22}) & \frac{1}{2}(\eta_{11}+\eta_{12}+\eta_{21}+\eta_{22}) & \frac{1}{\sqrt{2}}(\eta_{13}+\eta_{23}) \\ \frac{1}{\sqrt{2}}(\eta_{31}-\eta_{32}) & \frac{1}{\sqrt{2}}(\eta_{31}+\eta_{32}) & \eta_{33} \end{pmatrix}. \qquad (31)$$

The elastic potential energy is then written in terms of the η and the new equation of motion is determined. A similar procedure is used to align the a_1-axis with the [111] or the [221] propagation direction. The experimentally relevant equation of motion for either of these directions or for the general case is then found to be of the form

$$\rho\ddot{u} = \mu \frac{\partial^2 u}{\partial a^2} + \nu \frac{\partial u}{\partial a} \frac{\partial^2 u}{\partial a^2}, \qquad (32)$$

where μ is a combination of second-order elastic constants, and ν is a combination of second- and third-order elastic constants as defined by Holt (39).

It is conventional to write Equation (32) in the form

$$\rho\ddot{u} = K_2\left[\frac{\partial^2 u}{\partial a^2} + b \frac{\partial u}{\partial a} \frac{\partial^2 u}{\partial a^2}\right] + K_3\left[\frac{\partial u}{\partial a} \frac{\partial^2 u}{\partial a^2}\right], \qquad (33)$$

where K_2 is a linear combination of second-order elastic constants, and K_3, called the non-linearity parameter, is a combination of third-

order elastic constants. The parameter b is a constant whose value depends on the propagation and polarization directions, as do the values for K_2 and K_3. One notes that $\mu = K_2$ and $\nu = K_3 + bK_2$. Values for μ, ν, K_2, K_3, and b are given for sodium chloride in Table 2 of Holt's work (39). The particular propagation and polarization directions are specified in Table 2 by vectors referred to the crystal symmetry axes.

One might note from Equation (33) that the condition for "linear" behavior is not that K_3, the non-linearity parameter, be zero, but that $K_3 = -bK_2$. Thus, the fact that all of the third-order elastic constants of some material may vanish identically does not, in general, preclude second harmonic generation by finite amplitude acoustic waves propagating in the material. This fact is a consequence of the form of the elastic potential energy density $U(\eta)$ rather than the assumption of a non-linear stress-strain relationship.

The Solution to the Equation of Motion

Consider again the case of a longitudinal plane wave propagating in the [100] direction. It is found from Equations (23) and (32) that $\mu = C_{11}$ and $\nu = 3C_{11} + C_{111}$. Equation (32) then takes the form

$$\rho \ddot{u} = C_{11} \frac{\partial^2 u}{\partial a^2} + [3C_{11} + C_{111}] \frac{\partial u}{\partial a} \frac{\partial^2 u}{\partial a^2} . \qquad (34)$$

Since any second harmonic experimentally generated by the non-linearity of a crystal will be small in magnitude compared with the fundamental amplitude, we can assume that the solution u to Equation (34) can be written in the form

Table 2. Coefficients for the Equation of Motion for Sodium Chloride for Those Polarization and Propagation Directions Used

Propagation Direction	Polarization Direction	$K_2 = \mu$ x 10^{-12} dynes/cm.^{2}	$\nu = K_3 + bK_2$	
			K_3	bK_2 x 10^{-12} dynes/cm.^{2}
[100]	[100]	0.487	$1.000C_{111} + 0.000C_{112} + 0.000C_{144} + 0.000C_{166} + 0.000C_{123} + 0.000C_{456}$	1.461
[110]	[110]	0.431	$0.250C_{111} + 0.750C_{112} + 0.000C_{144} + 3.000C_{166} + 0.000C_{123} + 0.000C_{456}$	1.294
[111]	[111]	0.413	$0.111C_{111} + 0.667C_{112} + 1.333C_{144} + 2.667C_{166} + 0.222C_{123} + 1.778C_{456}$	1.239
[111]	[$\bar{2}$11]	0.163	$-0.079C_{111} + 0.236C_{112} - 0.236C_{144} + 0.236C_{166} - 0.157C_{123} + 0.157C_{456}$ $0.022C_{111} - 0.052C_{112} -$	0.000

Table 2. Coefficients for the Equation of Motion for Sodium Chloride for Those Polarization and Propagation Directions Used (continued)

Propagation Direction	Polarization Direction	$K_2 = \mu$ x 10^{-12} dynes/cm.^{2}	$\nu = K_3 + bK_2$	
			K_3	bK_2 x 10^{-12} dynes/cm.^{2}
[221]	$[\bar{1}\bar{1}5]$	0.140	$0.207C_{144} + 0.301C_{166} + 0.030C_{123} - 0.534C_{456}$	0.017

$$u(a,t) = u^{(0)} + u^{(1)} , \tag{35}$$

where $u^{(0)}$ is a solution to the linear equation, and $u^{(1)}$ is a small perturbation. We take the fundamental component of the solution to be

$$u^{(0)} = A_0 \sin (ka - \omega t) , \tag{36}$$

where A_0 is the wave amplitude at the fundamental frequency, k is the magnitude of the wave vector, and ω is the angular frequency of the acoustic wave, given by

$$\omega^2 = \frac{C_{11}}{\rho} k^2 . \tag{37}$$

Then $u^{(1)}$ is an approximate solution to the equation

$$\rho \ddot{u}^{(1)} = C_{11} \frac{\partial^2 u^{(1)}}{\partial a^2} + [3C_{11} + C_{111}] \frac{\partial^2 u^{(0)}}{\partial a^2} \frac{\partial u^{(0)}}{\partial a} . \tag{38}$$

Solving Equation (38) for $u^{(1)}$ yields

$$u^{(1)} = - \frac{3C_{11} + C_{111}}{8C_{11}} A_0^2 k^2 L \cos 2(ka - \omega t), \tag{39}$$

where L is the distance through which the initially sinusoidal disturbance has propagated. For a completely arbitrary choice of propagation and polarization directions, the equation of motion is represented by Equation (32). The analogous perturbation solution is then merely

$$u^{(1)} = - \frac{\nu}{8\mu} A_0^2 k^2 L \cos 2(ka - \omega t) . \qquad (40)$$

The magnitude of the second harmonic $u^{(1)}$ of Equation (39) or (40) can be experimentally determined by measuring the second harmonic content of a distorted acoustic wave. The sign of $u^{(1)}$ is determined by ascertaining the relative phase between the fundamental and second harmonic components.

The solutions to the equations of motion presented here are the same as those presented by Keck and Beyers (61), who were concerned with the case of a sinusoidal driver in a fluid. In their work an exact solution was presented for the particle velocity $v = \dot{u}$ in terms of Bessel functions and a discontinuity distance ℓ:

$$v(a,t) = 2v_0 \sum_{n=1}^{\infty} \frac{J_n(na/\ell)}{na/\ell} \sin n(\omega t - ka) . \qquad (41)$$

A power series expansion of Equation (41) yields the same perturbation term of Equation (40).

Determination of the Elastic Constants

Since the values for the second-order elastic constants are usually known, determination of ν in Equation (32) for a particular propagation and polarization direction combination yields a definite value for the corresponding linear combination of third-order elastic constants. Ideally, obtaining six different values for ν, corresponding to six different combinations of propagation and polarization directions, would enable one to determine all six of the discrete, third-order elastic constants for crystals of high cubic symmetry, such as sodium chloride. However,

as will be shown in the next section, it is not possible to find six combinations of propagation and polarization directions which will give six linearly independent equations involving the third-order elastic constants. Thus, we will combine our results of five linear combinations of the C_{ijk}'s with the assumption of the Cauchy relation $C_{144} = C_{456}$. This will then enable us to finally extract all six third-order elastic constants.

Since the magnitude of the second harmonic $u^{(1)}$ varies directly as the sample length L, it would be felicitous if $u^{(1)}$ continued to increase after reflection of the acoustic wave from the ends of the sample. Sample costs and physical size could both be significantly reduced, as several transits of the acoustic signal could be used to achieve a sizeable path length. Holt (39) has shown, however, that the process of second harmonic generation is exactly reversed after reflection of the acoustic signal from a stress-free boundary, which the sample-air interface represents. Thus, not only is there no additional production of second harmonic content in the returning signal, but also the distorted wave "undistorts."

For each particular propagation and polarization direction choice, one can measure the amounts of fundamental and second harmonic content of the acoustic signal, from which a value for ν_{exp} can be determined. We can write ν_{exp} as a linear combination of second- and third-order elastic constants

$$\nu_{exp} = p_1 C_{111} + p_2 C_{112} + p_3 C_{144} + p_4 C_{166} + p_5 C_{123} \qquad (42)$$

$$+ p_6 C_{456} + q_1 C_{11} + q_2 C_{12} + q_3 C_{44} ,$$

where the values of the p_i and the q_i are obtained by aligning the a_1-axis with the propagation direction as previously described. For N different experimental combinations of propagation and polarization directions, we obtain N values of K_3, given by

$$K_{3i} = p_1C_{111} + p_2C_{112} + p_3C_{144} + p_4C_{166} + p_5C_{123} + p_6C_{456}, \tag{43}$$

where i = 1, 2, 3,...,N. By combining Equations (42) and (43), we arrive at the system of equations

$$K_{3i} = \nu_{i\ exp} - q_1C_{11} - q_2C_{12} - q_3C_{44}, \tag{44}$$

where i = 1, 2, 3, ...,N. The C_{ij}'s are assumed to be known. Thus Equation (44) represents a set of N equations in six unknowns, the C_{ijk}'s. If Equation (43) includes six linearly independent combinations of the C_{ijk}'s, then Equation (44) can be solved for the complete set of all six third-order elastic constants.

One finds, however, that for all possible selections of propagation and polarization directions, the following relationship holds:

$$p_3 = 2\ p_5 + \frac{1}{2}\ p_6\ . \tag{45}$$

Using (45), we may rewrite (43) in the form

$$K_{3i} = p_{1i}C_{111} + p_{2i}C_{112} + p_{4i}C_{166} \tag{46}$$

$$+ (2C_{144} + C_{123})p_{5i} + (\tfrac{1}{2}\ C_{144} + C_{456})p_{6i}.$$

Thus, only the five quantities C_{111}, C_{112}, C_{166}, $(2C_{144} + C_{123})$, and $(\frac{1}{2} C_{144} + C_{456})$ can be determined by harmonic generation experiments.

The Five Constant Limitation

In order to derive Equation (45), let us consider a cubic medium in which the only strains used are single plane waves. Let us further consider only that portion Φ of the elastic potential energy density U which contains the particular third-order elastic constants C_{144}, C_{123}, and C_{456}:

$$\Phi(\bar{\eta}) = 2C_{144}[\bar{\eta}_{11}\bar{\eta}_{23}^2 + \bar{\eta}_{22}\bar{\eta}_{31}^2 + \bar{\eta}_{33}\bar{\eta}_{12}^2] \tag{47}$$

$$+ C_{123}\bar{\eta}_{11}\bar{\eta}_{22}\bar{\eta}_{33} + 8C_{456}\bar{\eta}_{12}\bar{\eta}_{23}\bar{\eta}_{31} .$$

As before in Equation (24) the bar superscript denotes a quantity measured with respect to the crystal symmetry axes. In general, however, the a_1 direction is along the propagation direction of the acoustic wave. By the rotation process previously described, the function Φ can be written

$$\Phi(\eta) = f_1C_{144} + f_2C_{123} + f_3C_{456} , \tag{48}$$

where the f_1 are functions of both the rotation matrix R and the strain elements.

If it can be shown that the equality

$$-2f_1 + 4f_2 + f_3 = 0 \tag{49}$$

holds for each rotation matrix R, then C_{144}, C_{123}, and C_{456} can only appear in Φ as $(2C_{144} + C_{123})$ and $(\frac{1}{2}C_{144} + C_{456})$. Then only the five quantities C_{111}, C_{112}, C_{166}, $(2C_{144} + C_{123})$, and $(\frac{1}{2}C_{144} + C_{456})$ can be determined by harmonic generation experiments.

For a plane wave of arbitrary polarization, the Jacobian matrix

$$J = \begin{pmatrix} 1 + \frac{\partial u_1}{\partial a_1} & 0 & 0 \\ \frac{\partial u_2}{\partial a_1} & 1 & 0 \\ \frac{\partial u_3}{\partial a_1} & 0 & 1 \end{pmatrix} \tag{50}$$

follows from Equations (15) and (19). The strain matrix, from Equation (6) is then given by

$$\eta = \begin{pmatrix} \eta_{11} & \eta_{12} & \eta_{13} \\ \eta_{12} & 0 & 0 \\ \eta_{13} & 0 & 0 \end{pmatrix}. \tag{51}$$

It is tempting to immediately put $\eta_{22} = \eta_{33} = \eta_{23} = \eta_{32} = 0$ into the expression for Φ. But the equations of motion given by Equation (17) contain $\frac{\partial U}{\partial \eta_{k\ell}}$, so that it might be possible for a term in f_i to vanish yet have a nonzero derivative. For a plane wave, however, only $\frac{\partial U}{\partial \eta_{1\ell}}$ appears, so that terms containing η_{22}, η_{33}, η_{23}, or η_{32} as a factor will not appear in the equations of motion.

Substitution for the f_i from Equation (47) into the left-hand side of Equation (49) yields the expression

$$-2f_1 + 4f_2 + f_3 = 4\bar{\eta}_{11}[\bar{\eta}_{22}\bar{\eta}_{33} - \bar{\eta}_{23}] \tag{52}$$

$$+ 4\bar{\eta}_{31}[\bar{\eta}_{12}\bar{\eta}_{23} - \bar{\eta}_{22}\bar{\eta}_{31}] + 4\bar{\eta}_{21}[\bar{\eta}_{32}\bar{\eta}_{13} - \bar{\eta}_{33}\bar{\eta}_{21}] .$$

Note that the right-hand side of Equation (52) is equal to four times the value of the determinant of the strain matrix, which is invariant under rotation of the coordinate system. From Equation (51) it is apparent that $\det(\eta) = 0$ in that particular coordinate system where a_1 is along the direction of propagation. Hence, $\det(\eta)$ must vanish in all rotated coordinate frames. We conclude that Equation (49) is true for all rotations R.

Attenuation Effects

As the fundamental and second harmonic signals propagate down the crystal, each undergoes a dissipation of acoustic energy, or attenuation. As an approximation to the problem of accounting for this attenuation, one assumes that the fundamental and second harmonic components of the acoustic signal are attenuated as if each were the only wave present. For the case of uniform attenuation, the fractional loss α per unit length of amplitude A is constant. For a layer of thickness da of the medium at a distance a from the origin, the fractional loss is given by

$$\frac{dA}{A} = -\alpha da . \tag{53}$$

Given the boundary condition that $A = A_0$ at $a = 0$, a solution to Equation (53) is

$$A(a) = A_0 e^{-\alpha a} , \tag{54}$$

where α, the attenuation factor, is in general, a function of frequency. Then the fundamental component of the acoustic wave is given by

$$u^{(0)} = A_0 e^{-\alpha a} \sin(ka - \omega t) . \tag{55}$$

Let α_1 = the attenuation factor for a wave of fundamental frequency f_1,

α_2 = the attenuation factor for a wave of second harmonic frequency $f_2 = 2f_1$ traveling alone in the medium,

A_1 = the amplitude of the fundamental at point a,

A_2 = the amplitude of the second harmonic at point a.

The change in the amplitude A_2 per unit path length is derived from a positive term, to account for the second harmonic generated by the fundamental, and a negative term, to account for the damping of the second harmonic. From Equation (40) we denote the change in A_2 as

$$\frac{dA_2}{da} = \frac{\nu}{8\mu} A_1^2 k^2 - \alpha_2 A_2 . \tag{56}$$

With the boundary condition that $A_2 = 0$ at $a = 0$, the solution to Equation (56) is

$$A_2(a) = \frac{\nu}{8\mu} A_0^2 k^2 \left[\frac{e^{-2\alpha_1 a} - e^{-\alpha_2 a}}{\alpha_2 - 2\alpha_1}\right] . \tag{57}$$

Thus the particle displacement u becomes

$$u(a,t) = A_0 e^{-\alpha_1 a} \sin(ka - \omega t) \tag{58}$$

$$- \frac{\nu}{8\mu} A_0^2 k^2 \left[\frac{e^{-2\alpha_1 a} - e^{-\alpha_2 a}}{\alpha_2 - 2\alpha_1} \right] \cos 2(ka - \omega t).$$

For the frequency range used in this work α_1 is taken to be equal to α_2, so that the amplitude of the second harmonic is

$$A_2 = \frac{\nu}{8\mu} A_0^2 k^2 \frac{e^{-\alpha a}}{\alpha} \left[1 - e^{-\alpha a} \right], \tag{59}$$

where $\alpha_1 = \alpha_2 = \alpha$. When we solve Equation (59) for ν and recall that $\nu = K_3 + bK_2$ and $\mu = K_2$, we find that K_3, the desired linear combination of third-order elastic constants, is given by

$$K_3 = -bK_2 - \frac{8K_2 A_2}{A_1^2 k^2 a} \left[\frac{\alpha a}{e^{\alpha a} - 1} \right]. \tag{60}$$

Finally,

$$K_3 = -bK_2 - \frac{2LA_2 K_2}{(\pi FT)^2 A_1^2}, \tag{61}$$

where L is the attenuation-adjusted sample length, F is the fundamental frequency, and T is the transit-time of a pulse down the sample.

Diffraction Effects

The circular quartz transducers are assumed to behave as piston acoustic sources. There exists a so-called Fresnel region in which the acoustic beam may be considered to be a plane wave. This zone extends from the transducer a distance of approximately r^2/λ, where r is the

radius of the transducer and λ is the wavelength of the wave in the solid. Beyond this distance, the ultrasonic beam diverges at an angle θ given by

$$\sin \theta = \frac{0.61\lambda}{r} . \tag{62}$$

This divergence manifests itself as an additional attenuation of the acoustic wave on the order of one decibel per r^2/λ. See Seki, Granato, and Truell (62).

For the sodium chloride samples used $r^2/\lambda \approx 20$ cm. Thus, the harmonic generation measurements were carried out in that region within the sample where the plane wave approximation is valid.

CHAPTER III

INSTRUMENTATION AND EQUIPMENT

Feasibility

The values of K_3 in Equation (33) may be calculated from knowledge of the displacement amplitudes of the sample at the fundamental and second harmonic frequencies and of K_2 from previous experiments in velocity measurement. A detector is then required for the measurement of strain amplitudes which can be accurately calibrated over a wide frequency spectrum. If one estimates values of the third-order elastic constants, one can calculate the expected amplitude of the second harmonic generated by the crystal sample for a specified fundamental vibration amplitude at a given frequency. The entire experiment becomes feasible if the choice of a detection apparatus permits the accurate measurement of these estimated second harmonic vibration amplitudes.

The selection of a frequency for fundamental operation requires the careful consideration of several factors. Diffraction of the acoustic wave results in an additional attenuation effect on the vibration amplitude and is a function of both sample dimensions and the acoustic wavelength. Seki, Granato, and Truell (62) determined that frequencies above 10 MHz were most desirable for the minimization of diffraction effects when using transducers of usual size.

The second harmonic vibration amplitude is seen in Equation (40) to be proportional to the square of the fundamental frequency, making

higher frequencies even more desirable. However, the cost and extreme fragility of quartz transducers cut for fundamental operation at frequencies above 60 MHz preclude the use of such transducers above that limiting frequency as sources for either longitudinal or transverse acoustic waves. Since I. F. Strips were readily available as high-gain amplifiers with passbands tuned respectively to 30 MHz and to 60 MHz, the choice of 30 MHz as the frequency of fundamental operation was optimal.

From Equation (40) one notes that the magnitude of the second harmonic amplitude will be at least one order of magnitude smaller that the fundamental amplitude. Since the fundamental displacements would be in the one-to-ten Ångstrom range, any choice of detector must be capable of yielding measurable signals for wave amplitudes down to 10^{-9} cm.

The end faces of the crystal sample will reflect the acoustic waves back and forth several times. These waves will interfere with each other on each pass, until their energy is dissipated through attenuation. This interference is undesirable and its presence suggests using pulsed acoustic waves in the experiment. The repetition rate of the initial electric signal must be chosen to allow one pulse train to die out before the next pulse is introduced. One must also keep in mind that, since the receiving end of the crystal is a force-free end, the displacement amplitude there will be twice the magnitude of the displacement amplitude within the body of the sample.

Capacitance Microphone Detector

Sampleholder

A diagram of the mechanical parts of the capacitance microphone detector sampleholder assembly is shown in Figure 1. The crystal rests vertically on the annular portion of the bottom plate assembly, which serves as electric ground for the detector circuit. The copper center button of the bottom plate is the detecting electrode and is held in place by epoxy resin, which also serves to isolate the button electrically from the grounded outer ring. This button is recessed slightly below the plane of the annular plate so that the sample end face and the copper button form the components of a parallel plate capacitor. When a bias voltage is applied to the center electrode, a uniform electric field is set up across the capacitor gap. Plane, longitudinal acoustic waves, impinging on the sample face, cause the gap spacing to oscillate about some equilibrium value, producing a time-varying voltage between the center button and the ground plate.

As a source for the generation of longitudinal acoustic waves, a piezoelectric transducer was affixed to the upper end of the sample with a suitable bonding material. A copper electrode, flat on one side, provided the electric signal to the transducer and was held tightly in place by a spring mount. To complete the transducer assembly, the copper outer ring was grounded, like its lower twin, and the entire assembly held in place atop the sample with flexible bands. Both ends of the crystal were metallically coated, since sodium chloride is a non-conductor. Careful placement of the upper and lower assemblies with respect to the gold coatings, which also served to assure good electrical shielding,

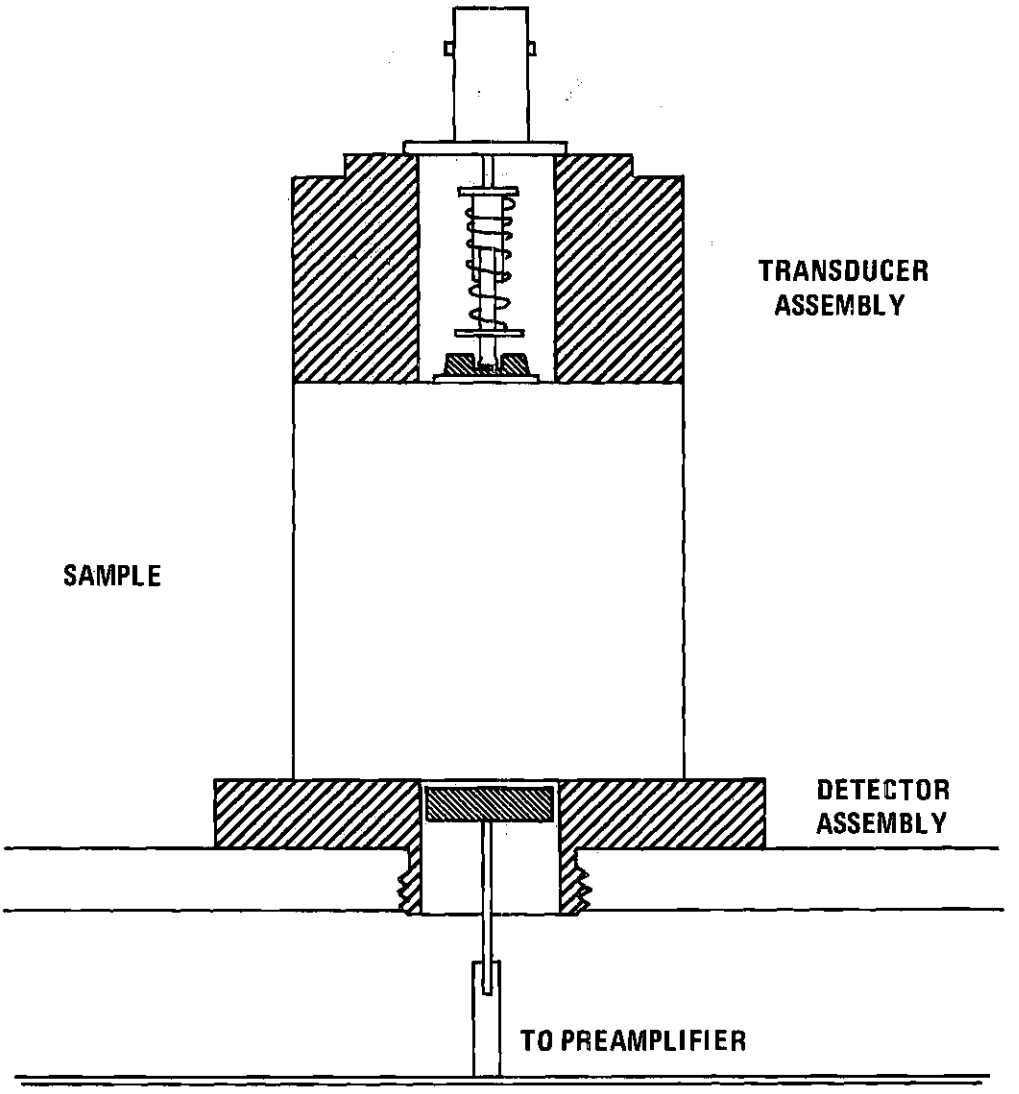

Figure 1. Capacitance Microphone Detector and Sampleholder Assembly

was absolutely necessary for the retrieval of the ultrasonic signals. Finally, the electrical input to the upper assembly was by means of a B. N. C. connector, whose center pin was connected to the copper center electrode, which rested on the transducer itself.

In order to achieve maximum sensitivity of the capacitance microphone detector, the gap spacing had to be made as small as possible, which will also be discussed in the next section. To this end, both the sample faces and the mating surfaces of the detector assembly were lapped until optically flat. The desired gap spacing was then created by masking the copper center button of the detector assembly with tape and electroplating copper onto the annular ring by immersion of the assembly in a standard copper bath until the thickness of the copper so deposited was slightly greater than desired. The outer ring was then lapped until the final gap spacing was reached. Care was taken to maintain parallelism between the outer ring and the inner copper button. To check for parallelism, an optical flat can be placed on the detector assembly and illuminated with monochromatic light, as from a sodium lamp or laser. If the fringe patterns so produced are identical in density and relative orientation over both ring and center button, then the two parts are truely parallel.

Rather than measure this gap spacing directly, the gap capacitance was determined with the sample in place on the detector assembly using a digital capacitance meter. The subtraction from this capacitance value of the capacitance of the lead wires with the sample removed thus enables one to determine accurately the gap capacitance. From this gap capacitance the gap spacing is directly determined. Gap spacings on the order of ten microns were measured in this manner.

Preamplifier

The capacitance microphone detector and preamplifier circuits were combined on a single printed circuit board, as shown in the schematic diagram of Figure 2. The output impedance of the preamplifier was chosen to match both the 50 ohm impedance of the RG59/U coaxial cable and the input impedance of the high gain amplifiers. The time-varying gap capacitance is represented in the diagram by a variable capacitor. Typical quiescent values for this capacitance lie between 20 and 30 picofarads. The design and physical layout of the actual circuit were generally the same as those of Gauster (63). Because of the proximity of a television broadcasting antenna using frequencies around 60 MHz, it was essential that both the detector and preamplifier be heavily shielded from outside electromagnetic interference. For this reason the preamplifier circuit board and detector lead wires were mounted inside a brass container. All coaxial wires leading into the box were also shielded by metal, also brass.

One may determine the displacement amplitude A of the sample face from the various circuit parameters. If we represent the input impedance of the preamplifier with a resistor, R_2 = 38 kilohms, the detector circuit can be represented as shown in Figure 3. It follows from a straightforward analysis of the circuit that the time-varying voltage V produced by a sinusoidal displacement A of the sample face is

$$V = \frac{R_2 C_0 V_0 \omega \gamma \left[1 + (C_0/C_2)^2 (R_2 C_0 \omega)^{-2}\right]^{1/2}}{\left[(1/R_1 C_2 \omega - R_2 C_0 \omega)^2 + (1 + C_0/C_2 + R_2/R_1)^2\right]^{1/2}}, \qquad (63)$$

where C_0 is the quiescent value of the gap capacitance, V_0 is the applied

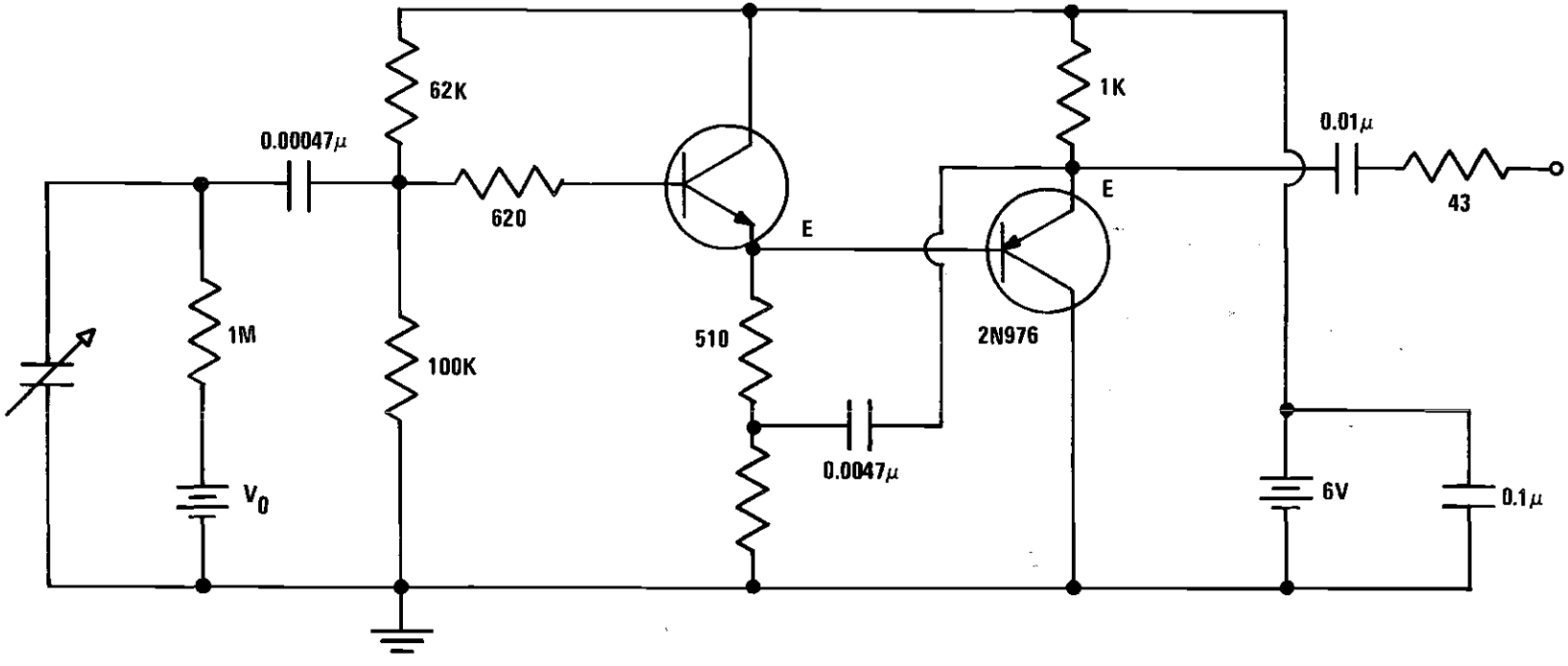

Figure 2. Schematic Diagram of Detector and Preamplifier Circuit

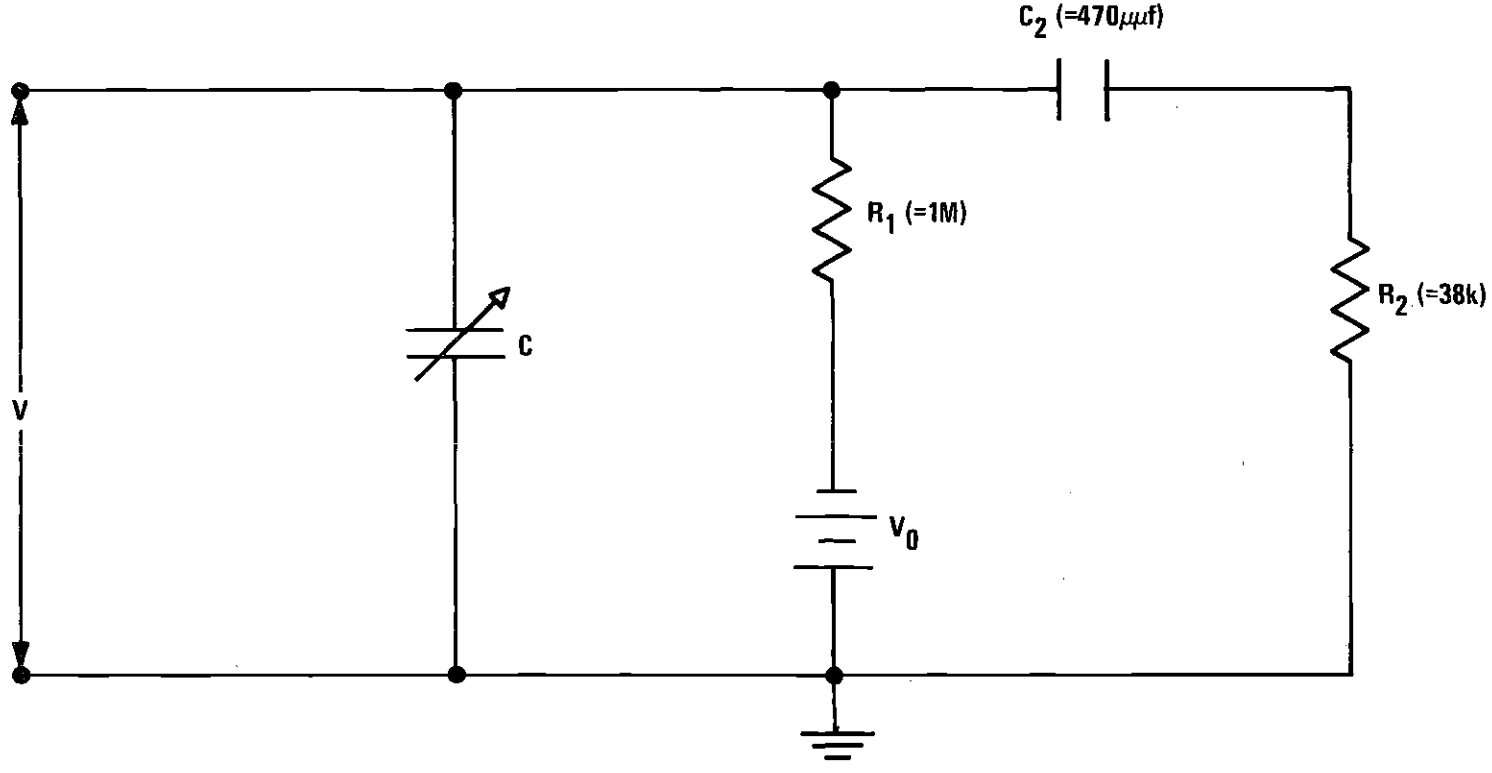

Figure 3. Input Equivalent Circuit of Detector and Preamplifier

bias voltage, $\gamma = A/s_0$ is the ratio of the displacement amplitude A to the quiescent gap spacing s_0, ω is the angular frequency of vibration, and the other quantities are the various parameters of the circuit as shown in Figure 3. With typical values for these parameters of $C_0 = 25$ pf, $C_0/C_2 = 0.05$, $R_2/R_1 = 0.04$, $R_1C_2\omega = 9 \times 10^4$ rad., and $R_2C_0\omega = 180$ rad. for a frequency of 30 MHz, Equation (63) simplifies to the convenient form

$$V = \gamma V_0 \tag{64}$$

to an error of less than 0.5 per cent. A derivation of Equation (63) is found in Appendix A, as is a discussion of the harmonic generation limitations of the capacitance microphone detector itself.

The gain of the preamplifier is, of course, a function of signal frequency. The frequency response of the circuit, as shown in Figure 4, was found by Gauster to be flat within the region of interest. This frequency range of constant gain extends from about 5 MHz to 90 MHz. Using the standard definition of bandwidth as the frequency interval between the minus 3 dB. points, the bandwidth is seen to be 130 MHz. Here 0 dB. relative gain corresponds to an actual gain of 0.49 dB. With this size bandwidth, the rise time of the preamplifier is about 3 nanoseconds, providing excellent pulse response.

From Equation (64) it can be seen that the signal voltage is merely the product of the ultrasonic displacement amplitude A and the electric field intensity produced by the bias voltage across the gap. Thus, any practical limitation on signal strength is determined only

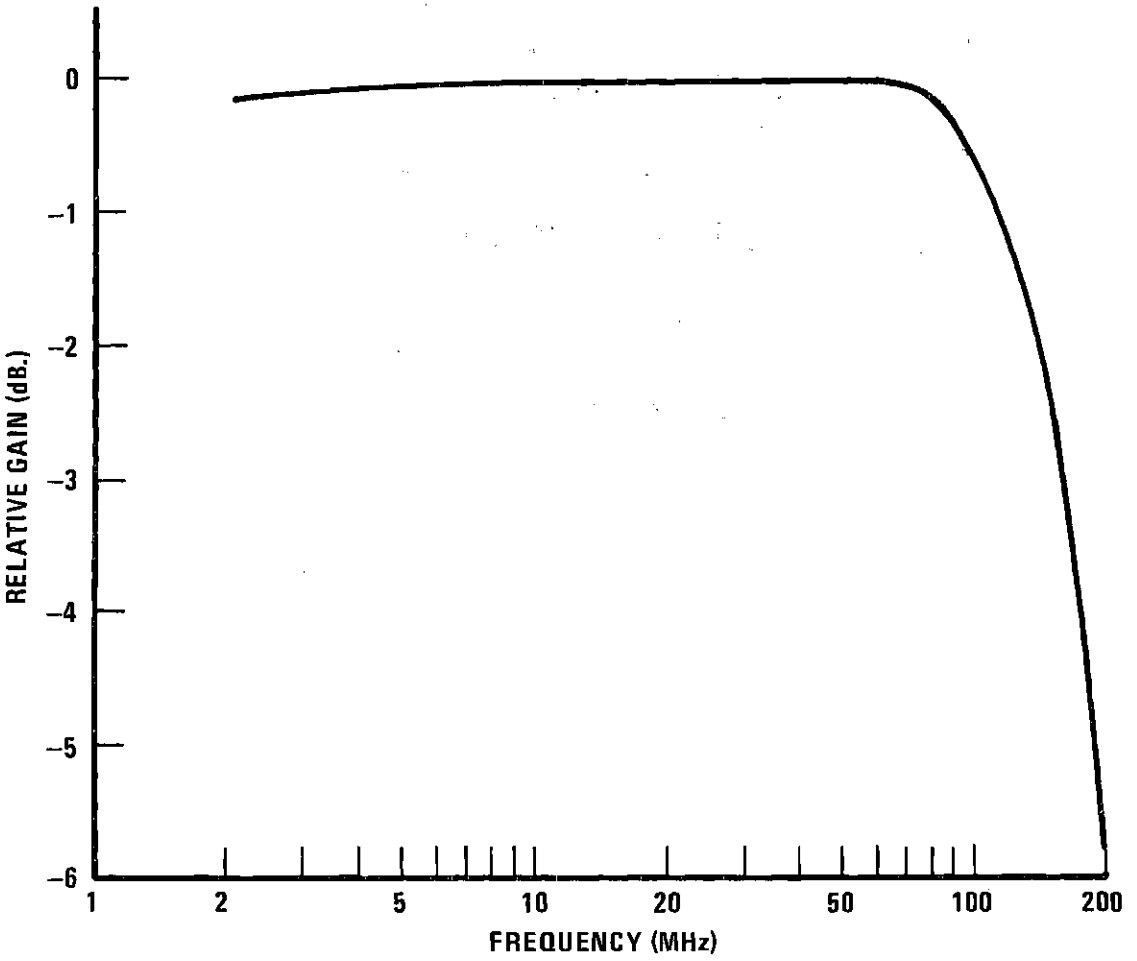

Figure 4. Frequency Response of Preamplifier Circuit

by the breakdown field of the air in the gap. Kisliuk (64) has shown that the breakdown field of air is several million volts/cm. at atomospheric pressure for gap spacings of less than 1 micron. By carefully polishing the copper surface of the detector button and the sample end face, fields of 110 KV/cm. were obtained with gaps of 20 microns. Lattice displacements on the order of 10^{-9} cm. with this gap spacing and a bias voltage of 220 volts yielded signals on the order of 100 microvolts. With judicious choice of the transistors used in the preamplifier and careful shielding, noise could be held to about 10 microvolts, RMS, so that the signal-to-noise ratio was favorable.

Magnetic Detector

Figure 5 is a diagram of the mechanical parts of the magnetic detector and sampleholder assembly. The sample lies horizontally, with the acoustic pulses traveling down the crystal axis, between the poles of an electromagnet. The detector consists of two copper contacts which are spring mounted by phosphor-bronze supports. These contacts rest against opposite ends of a gold strip which is evaporated onto the sample end face. As a plane, transverse ultrasonic wave impinges on the sample end face, the gold strip is caused to vibrate, inducing an electromotive force along the strip. Since the wavelength of the ultrasonic waves is on the order of 10^{-4} meter, and the thickness of the evaporated gold strip is but a few thousand Ångstroms at most, the lattice vibrations should be unperturbed by the presence of the gold. The time-varying voltage is picked up by copper contacts and transmitted directly to the high gain amplifiers.

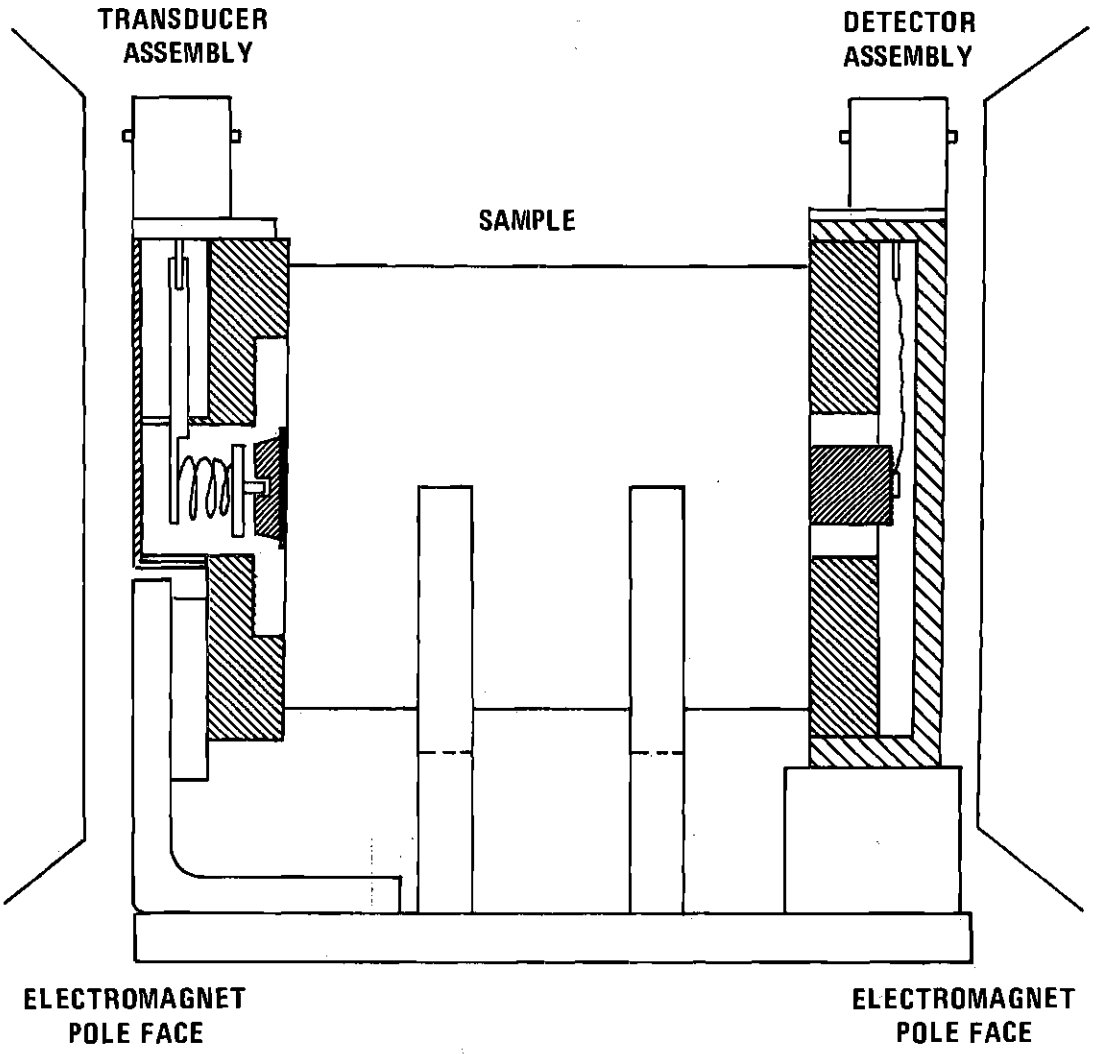

Figure 5. Magnetic Detector and Sampleholder Assembly

A great advantage which the magnetic detector has over the capacitance microphone detector is that the magnetic detection technique can be used to determine both longitudinal and transverse displacements, while the capacitance microphone technique is necessarily restricted to measurements of longitudinal displacements. By rotating the crystal sample so that the evaporated gold strip, when vibrating with the sample, cuts lines of magnetic flux, one can easily measure transverse acoustic displacements, in addition to being able to determine longitudinal motion. The use of second harmonic generation to determine third-order elastic constants in solids has heretofore been restricted to longitudinal acoustic waves. Thus, this magnetic detector permits a new method of attack.

The signal input to the transducer is essentially the same as that used in the capacitance microphone assembly, where the differences are purely configurational, due to the space limitations imposed by the pole separation of the magnet. The assembly is built around a copper ring, through which a spring loaded contact provides the signal to the transducer. A B. N. C. jack mounted radially to the ring allows attachment of doubly-shielded RG9/U coaxial cable from the pulsed oscillator. The outer ring is electrically grounded and isolated by air from the center contact. The center conductor, in turn, fits into a copper button, which rests against the quartz transducer, allowing maximum contact.

An AC-cut quartz transducer, cut for shear mode vibration at 30 MHz, was permanently bonded onto the gold-evaporated sample face with a mixture of Duco Cement and acetone. This type of solid bond is

necessary, since a viscous bond such as Nonaq will not support shear vibration.

The sample rested on plastic supports glued to a plastic base. The use of plastic and nonmagnetic metals, such as aluminum and copper, was required in order to keep the magnetic field in the vicinity of the detector electrodes as uniform as possible. All screws used in the construction of the assembly were either brass or stainless steel, for the same reason. The aluminum supports of the transducer assembly allowed variation of the height of the input contact according to the diameter of the sample being used.

Each of the copper pickups was soldered to phosphor-bronze supports, which allowed the contacts to bend freely and to give maximum contact with the gold strip on the sample face, while minimizing damage to the gold by the pressure of the sharp copper edges. One of the pick-ups was connected directly to ground, while the other was soldered to a B. N. C. output jack. Again RG9/U doubly shielded coaxial cable was used to connect the detector output to the amplifiers in an effort to keep out extraneous electrical noise.

The induced Emf in the gold strip is given by Faraday's law

$$E = \int (\vec{B} \times \dot{\vec{u}}) \cdot d\vec{\ell} \ , \tag{65}$$

where $\vec{B}$ is the magnetic field strength vector, $\dot{\vec{u}}$ is the velocity of a point on the sample end face, and $d\vec{\ell}$ is an increment of length of the gold strip. Since the displacement amplitude is sinusoidal, the magnitude of the induced voltage is just

$$E = Bu\ell\omega \ , \tag{66}$$

where ω is the angular frequency of the signal. Thus, the amplitude of the ultrasonic displacement is just

$$A = \frac{E}{2\pi B \ell F} \ . \tag{67}$$

Instrumentation

The equipment used for this research consisted basically of a pulsed oscillator, one of the two detection devices previously discussed, amplifiers, and readout devices to measure low amplitude ultrasonic pulses in single crystal sodium chloride. The instrumentation was generally similar to that used by Gauster (63) for the capacitance microphone detector. A block diagram of the experimental arrangement using the capacitance microphone is shown in Figure 6. An analogous block diagram, shown in Figure 7, describes the arrangement using the magnetic detector.

The pulse source was a pulsed oscillator, model PG-650C (Arenberg Ultrasonic Laboratory, Inc.). This oscillator provided pulses of variable width and intensity over a range of frequencies by the substitution of appropriate oscillator coils. Repetition rate of the pulses was adjustable so that samples of different lengths could be used in the experiment, if required.

Attenuation for calibration purposes was provided by two continually variable precision attenuators, models 3132 and 3162 (Airborne Instruments Laboratory). A simple matching network provided the proper

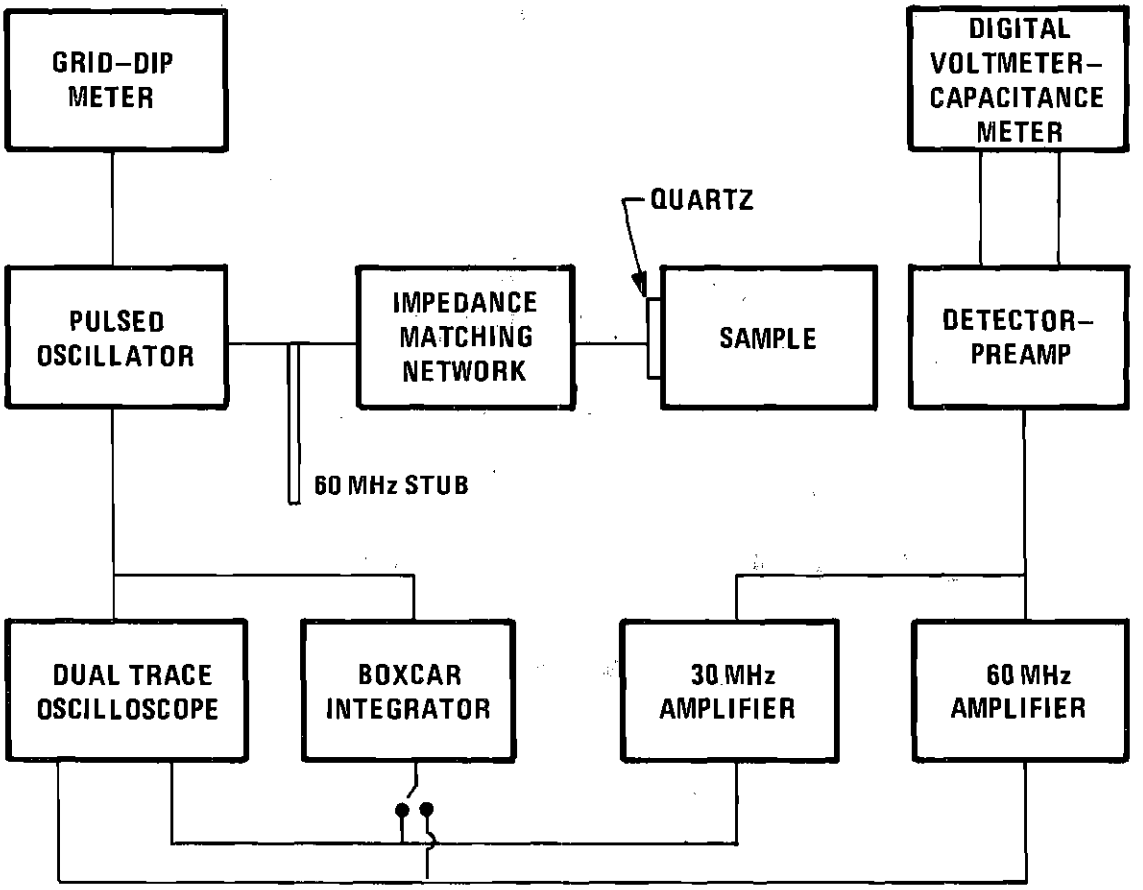

Figure 6. Block Diagram of Amplitude Measuring System Using the Capacitance Microphone Detector

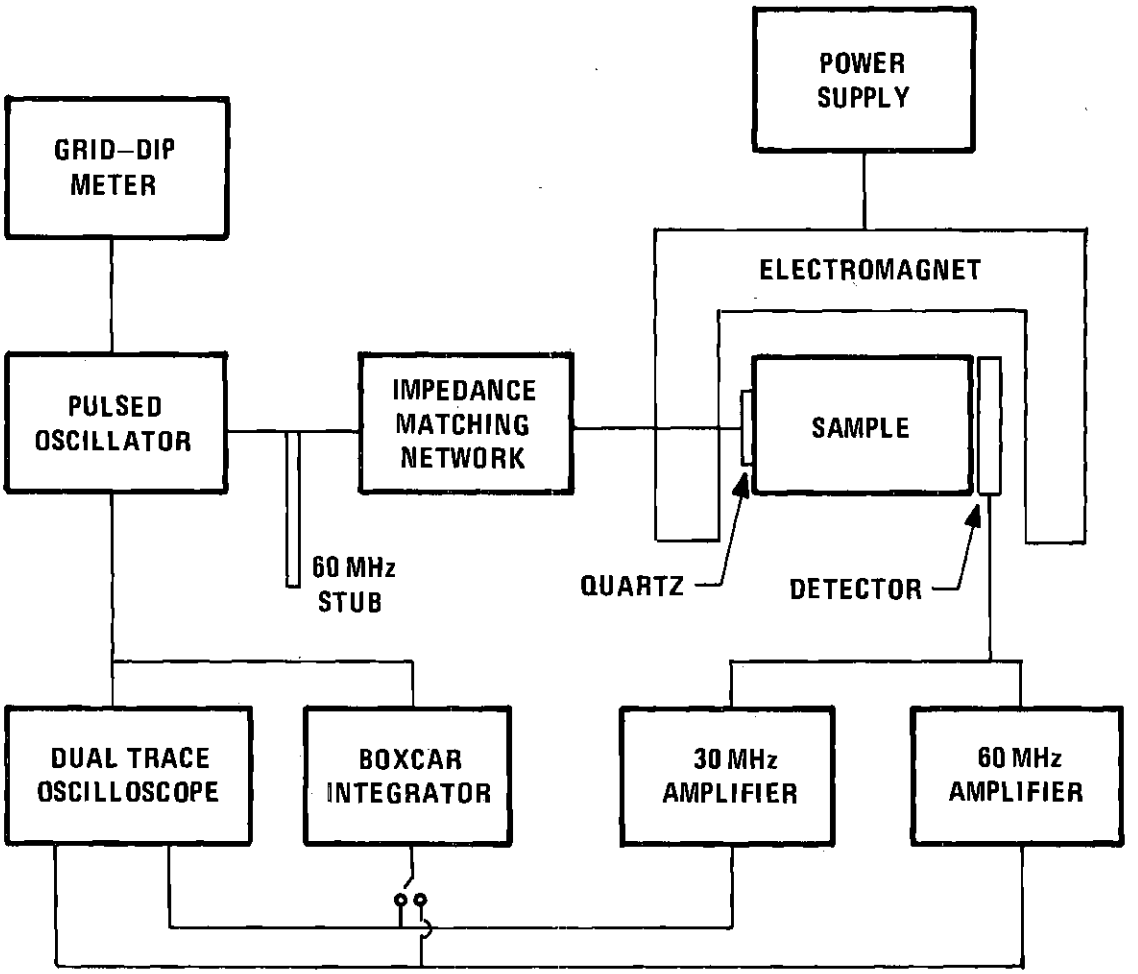

Figure 7. Block Diagram of Amplitude Measuring System Using the Magnetic Detector

impedance matching between the 95 ohm output impedance of the pulsed oscillator and the 50 ohm impedance of the attenuators. The attenuators were tuned to 30 MHz and 60 MHz respectively and had a range of over 110 dB .

The DC bias potential required in the detector-preamplifier was obtained from a voltage regulated power supply, model ABC 1000M (Kepco, Inc.), which provided bias voltages continuously variable from zero to 1000 volts. The exact voltage magnitude was monitored with a digital voltmeter plug-in unit, model DP-100 (Hickock Electrical Instruments Company) with its mating mainframe, model DMS-3200.

The same mainframe was also used to determine the capacitance of the gap spacing of the microphone detector. A capacity meter plug-in unit, model DP-200, enabled measurement of this capacitance to one picofarad accuracy.

To monitor the frequency of the output of the pulsed oscillator, a grid-dip meter, model 59 (Measurements Corporation) was employed. The grid-dip meter itself was calibrated against an electronic counter and frequency converter plug-in unit, models 5245L and 5253B respectively (Hewlett Packard). The calibration of the grid-dip meter was done in continuous mode operation using the frequency counter, but the pulse response of the grid-dip meter would be the same as the CW response.

Up to 100 dB . gain was provided by tuned amplifiers, models EV3010 and EV6010 (RHG Electronics Lab) with center frequencies at 30 MHz and 60 MHz respectively. Each amplifier had a passband adjusted to 10 MHz, which was large enough to reproduce pulses of short duration. Power to both amplifiers was supplied by a single voltage regulated power supply, model KR12M (Kepco, Inc.).

The rectified video output of both amplifiers were observed on a model 585A oscilloscope with a type 82 dual-trace plug-in unit (Tektronix, Inc.). Triggering of the oscilloscope was supplied by a trigger pulse generated at the pulsed oscillator at the same time that the leading edge of the signal pulse was created.

Accurate pulse height measurement was accomplished with the use of a model CW-1 boxcar integrator (Princeton Applied Research), which allowed the retrieval of signals as small as 0.1 volts buried in noise of several volts RMS. The pulsed oscillator also triggered the integrator gating, whose width and position in time were both adjustable.

The only differences in instrumentation in adapting the experiment to magnetic detection were those involving the detector itself and the electromagnet. See Figure 7. A four-inch diameter, adjustable electromagnet, model 7536-modified (Alpha Scientific Laboratories, Inc.) was used to provide a uniform magnetic flux density up to a maximum value of one-half weber/m^2. The current to the magnet windings came from a 20 ampere, 100 volt adjustable power supply, model AL100, and regulator, model AL104R (Alpha Scientific Laboratories, Inc.). Monitoring of the magnetic field strength was made by calibrating the current dial reading of the power supply with the magnetic field with a model 620 gaussmeter (F. W. Bell) for each position of the detector between the pole pieces.

CHAPTER IV

EXPERIMENTAL PROCEDURE

Sample Preparation

The single crystals of sodium chloride which were used in this experiment were obtained from the Harshaw Chemical Company. Each crystal was cylindrical, 3.8 cm. long and 2.5 cm. in diameter, with the cylinder axis along a specified crystalline direction. Both faces of the cylinder were cut at right angles to the axis and were polished optically flat. Ultrasonic measurements were made on four crystals, whose axes were oriented in the [100], [110], [111], or [221] crystallographic direction. This choice of directions was dictated by two factors: the cost of obtaining single crystals of sodium chloride of this shape and size and the fact that this selection of crystals was sufficient to yield the five combinations of third order elastic constants which were sought.

To reduce the appreciable attenuation of the ultrasonic waves in the crystals, it proved advantageous to anneal each of the samples in an oven in an attempt to relieve the thermal stresses set up within the lattice in the actual formation of the crystal. Each sample was heated within the oven at a controlled rate of 60 C° per hour until the temperature of the oven stabilized at 540° C. After half an hour at this temperature, the sample was allowed to cool to room temperature at a rate of 60 C° per hour. Since the melting point for sodium chloride is 801° C, no deterioration of the crystal resulted from the annealing

process. All crystals so treated showed significant reduction in the amount of attenuation of ultrasonic waves.

To properly orient the direction of the AC-cut quartz transducer onto the sample face for generation of transverse mode acoustic waves, it was necessary to locate as accurately as possible particular vectors directions in two of the crystals: the $[\bar{2}11]$ direction in the [111] crystal and the $[1\bar{1}5]$ direction in the [221] crystal. Although the latter two directions are not perpendicular to each other, they are as close as it was possible to get considering Holt's tabulation of propagation and polarization directions for acoustic waves in sodium chloride (39). These particular vectors were located using standard Bragg reflection of neutrons. This orientation was carried out with the assistance of D. E. Wrege and J. W. Lynn using one Angstrom neutron beams at the Frank H. Neely Nuclear Research Center on the Georgia Tech campus.

A thin coating of gold was then evaporated onto the transducer face of the sample using a vacuum evaporator (Veeco Instruments, Inc.). A layer several thousand Angstroms thick was sufficient to act as a ground plate for the signal input assembly and transducer. For use with the capacitance microphone detector, the opposite end of the sample was also completely coated with a gold layer of comparable thickness. For use with the magnetic detector, the opposite face was masked, allowing the deposition of a gold strip about 1.5 cm. long.

When the gold layer or strip became worn from repeated handling, the gold was removed with acetone. The surface was relapped with first a #30-1/2 grit and then a #38-1200 grit (U. S. Products Company) before gold was again evaporated onto the surface. The same lapping compounds

were used to polish all copper surfaces which were in contact with the sample faces.

Amplitude Measurements

A pulsed oscillator furnished high voltage electrical signals at 30 MHz up to 600 volts peak-to-peak with pulse widths in the 5 to 10 microsecond range. A tuned matching network provided both step-up transformer capability and clean, squared pulse shape. A schematic diagram of this network is shown in Figure 8. The network was basically a series combination of an autotransformer of inductance

$$L = L_1 + L_2 \tag{68}$$

and capacitance

$$C = C_1 + C_2 , \tag{69}$$

where C_1 was a small variable capacitor of approximately 100 pf., and C_2 was the capacitance of the quartz transducer in place of the sample. The inductance L of the coil was about 0.5 microhenries. Varying the ratio L_1/L_2 allowed additional amplification of the electrical signal from the oscillator. The variable capacitor C_1 was then adjusted to series resonance at the frequency of operation and also allowed tuning the circuit for optimal pulse shape. The Q of the resonant circuit was determined by the resistor R, whose value was 50 ohms in this experiment.

The pulsed electrical signal was then applied to the transducer, a quartz disc, X-cut for longitudinal vibration, or AC-cut for transverse vibration. Those transducers used were either 1/2 inch or 3/4

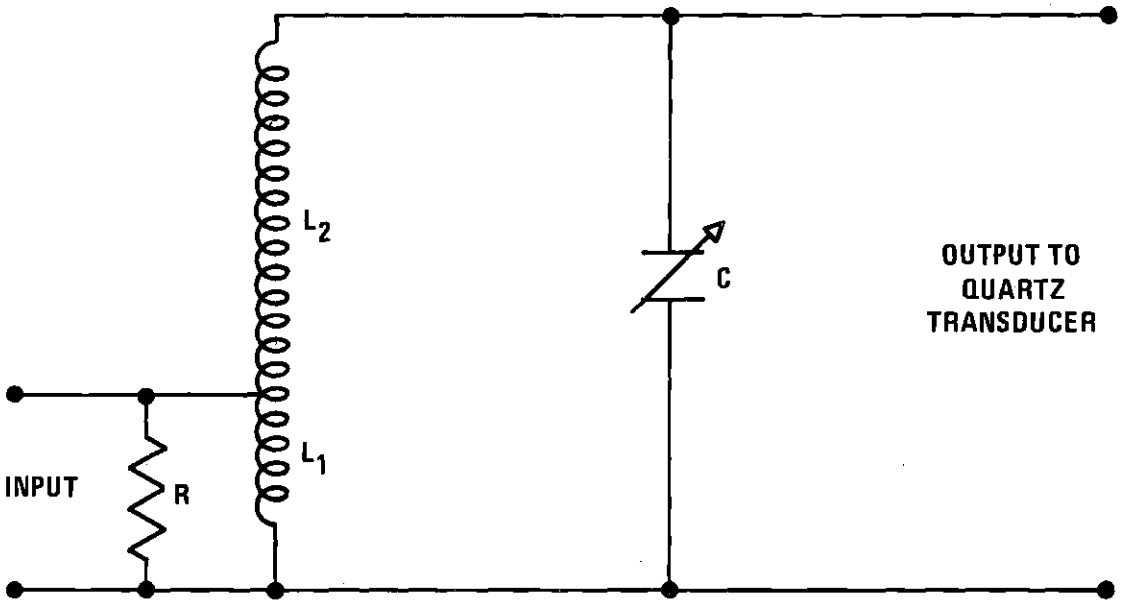

Figure 8. Impedance Matching Network

inch in diameter and fine ground polished for fundamental mode operation at 30 MHz. Both gold plated and unplated transducers were used, with neither showing any apparent advantage over the other (Fisher Scientific Company). It was found that Nonaq stopcock grease provided a suitable bond between the transducer and the sample face for X-cut transducers. For transverse acoustic wave generation, however, use of the Nonaq was not feasible, as a shear wave will not propagate through such a viscous medium. A suitable bonding material was fabricated by diluting Duco cement (E. I. du Pont de Nemours & Company) with sufficient acetone to make the mixture flow freely. A small drop of this diluted glue was applied to the sample face and the AC-cut transducer quickly positioned before the acetone evaporated. When all the acetone had evaporated, the resulting solid bond proved to support shear waves adequately.

For either detection technique, the ultrasonic pulses were detected at the opposite end of the sample after passing down the full length of the crystal. Echoes of the original pulse resulted from repeated reflections from the sample end faces. Occasionally the first returning pulse would be of sufficiently large magnitude to cause the transducer to vibrate resonantly, thus producing an additional electric wave. However, these electric pulses could be distinguished from the acoustic pulses by the position of each within the pulse train, as displayed on the oscilloscope screen. The electrical pulses occurred exactly halfway in time between the detection of acoustic pulses, since they were produced at opposing ends of the sample. Since the first pulse in the train was the initial electrical pulse, it was then a simple task to determine the source of every other pulse.

This characteristic pattern of electrical and acoustic pulses and echoes is shown in Figure 9, which shows the oscilloscope screen displaying the video output of both amplifiers. The upper trace is the 30 MHz channel, and the 60 MHz channel is on the lower trace. Note that the initial electrical pulse in the 30 MHz pattern is absent in the 60 MHz pattern, further indicating a spectrally pure initial signal. Numbering the pulses from left to right, the even-numbered pulses are acoustic, while the odd-numbered ones are electric. Accurate measurement of the pulse heights themselves was facilitated by the use of a boxcar integrator, which time-averaged a single repetitive signal, thus cancelling the effects of random noise.

With the high gain of the amplifiers, typically about 70 dB. for the 30 MHz channel and 100 db. for the 60 MHz channel, video signals of up to twenty volts in magnitude were recorded. The gain of the 60 MHz amplifier was adjustable, as the negative DC level of one of the grids of each of the amplification tubes could be varied (with batteries) as a manual gain control. This proved to be useful when recovering particularly small signals otherwise buried in electrical noise.

Calibration Procedure

During a run using the capacitance microphone detector, one recorded the bias voltage necessary to yield a pulse height of a given magnitude on the boxcar integrator. This procedure was followed on both the 30 MHz channel and the 60 MHz channel for a single setting of the pulsed oscillator output. A complete run then consisted of bias voltage readings and pulse height readings for a range of oscillator

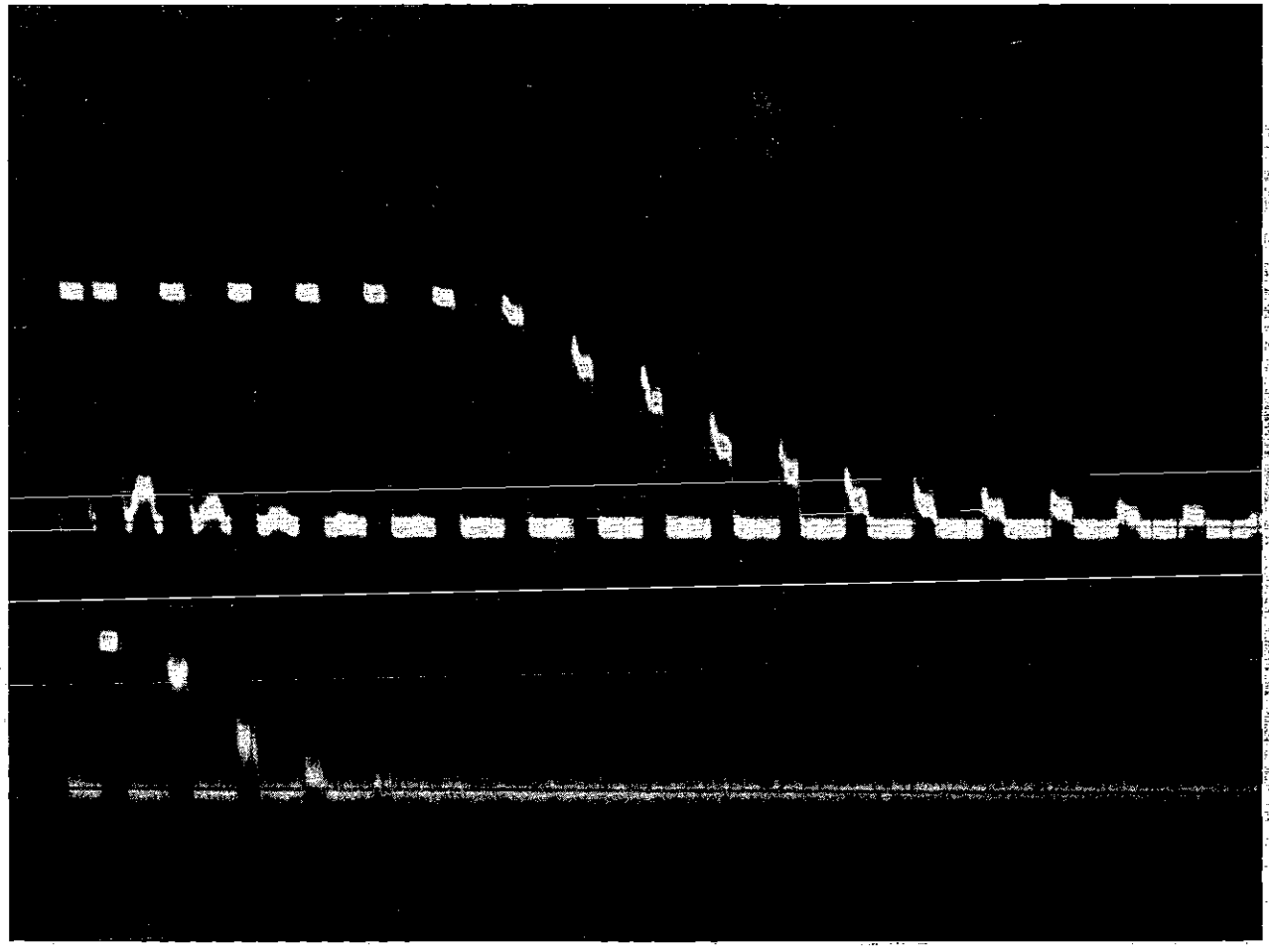

Figure 9. Oscilloscope Traces of Detected Signals at 30 MHz (Upper) and at 60 MHz (Lower)

strengths. At the end of each run the gap capacitance was recorded, along with the detector button area, the frequency of the fundamental signal, the length of the sample crystal, and the transit time of the pulse down the sample. As noted in the discussion on attenuation in Chapter II, measurement of the relative heights of the first acoustic pulse and the first echo yield a value for the attenuation constant α of the ultrasonic signal. Sample data sheets are shown in Appendix B.

When using the magnetic detection apparatus, one recorded the current dial reading of the power supply to the electromagnet and the distance between the detector pick-ups, in addition to those parameters pertinent to this apparatus. The current dial reading, and the magnetic field intensity to which it is calibrated, is the analogous parameter to the bias voltage reading of the capacitance microphone technique. Using either method of detection, the intensity of the oscillator signal was decreased incrementally, and data recorded at each setting. It was anticipated that the combination of third-order elastic constants derived from each set of readings remain a constant as the wave vibrations were made smaller and smaller.

After a complete set of readings had been recorded, both amplifiers were carefully calibrated. This calibration was accomplished by applying an electrical signal of precisely known value to the inputs of both amplifiers first at the fundamental frequency and then at the second harmonic frequency. Figure 10 shows a schematic diagram of the general calibration procedure. The amplitude of each calibration signal was then adjusted so that the same pulse height was obtained on the boxcar integrator as was obtained during the preceding run. At this point the calibration voltage magnitude is equal to that of the

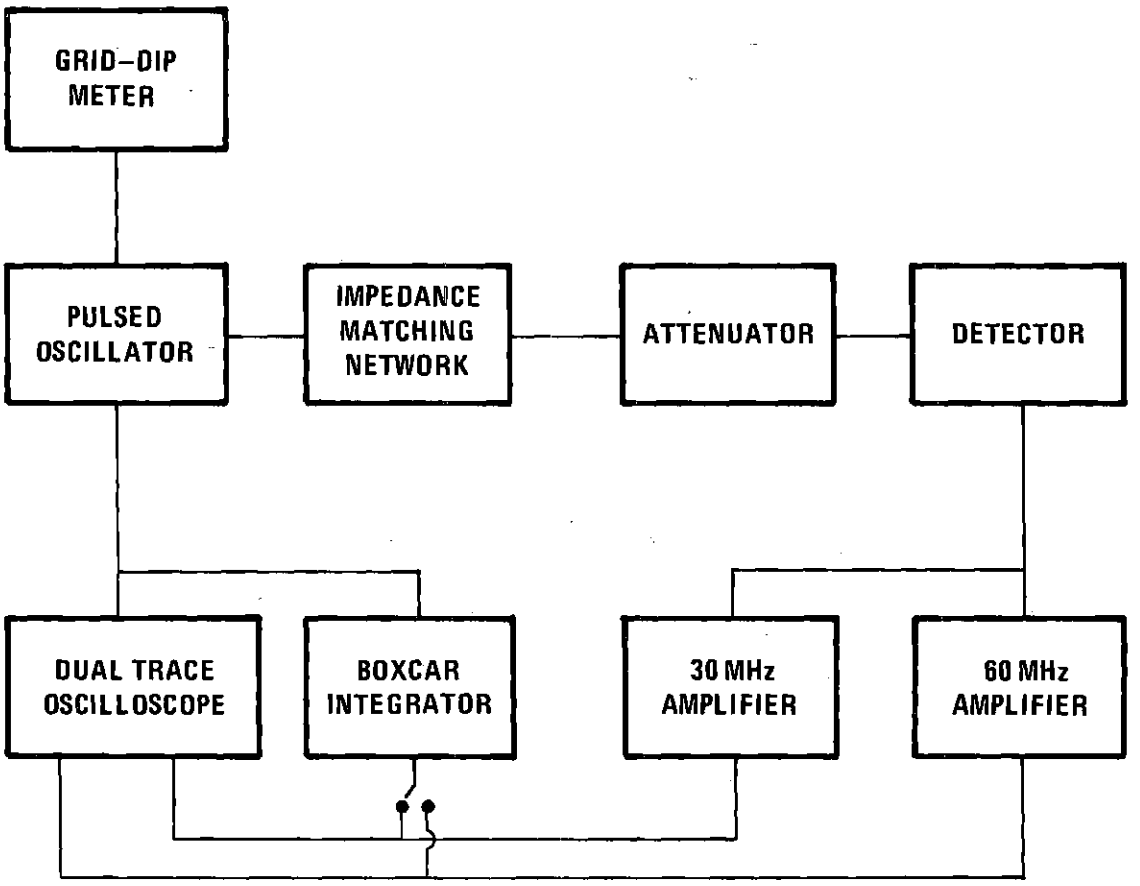

Figure 10. Block Diagram of the Calibration System

electrical signal created by either of the detectors due to vibration of the sample end face. Application of Equation (64) for the capacitance microphone, or Equation (67) for the magnetic detector, then yields the absolute amplitude of the ultrasonic displacement. It must be observed, however, that since the end face of the sample represents a stress-free boundary between the crystal and air, the vibrational amplitudes at the detector will be twice the magnitude as those within the body of the sample itself. This factor of two must be taken into account in the calculation of the absolute amplitudes used in the derivation of each value for K_3.

A pulsed signal, like the one used during a run, was obtained from the oscillator at either 30 MHz or 60 MHz and was connected to a two resistor impedance matching network, a schematic diagram of which is shown in Figure 11. The 95 ohm output impedance of the pulsed oscillator was thus properly matched to the 50 ohm impedance of either of the precision attenuators. The output of an attenuator was connected to the input jack of the oscilloscope, which was terminated with a 50 ohm resistor to simulate the input impedance of the amplifiers. With an attenuator set arbitrarily at zero dB., the calibration voltage was adjusted to some convenient value, such as 0.5 volt, by direct comparison with a calibrated square wave internally generated within the Taktronix oscilloscope. The terminating resistor was then removed, and the attenuation increased before the attenuated signal was applied to either the preamplifier or amplifier input. The amount of attenuation was carefully adjusted until the pulse height of the amplifier output as measured on the boxcar integrator was the same as that during a run.

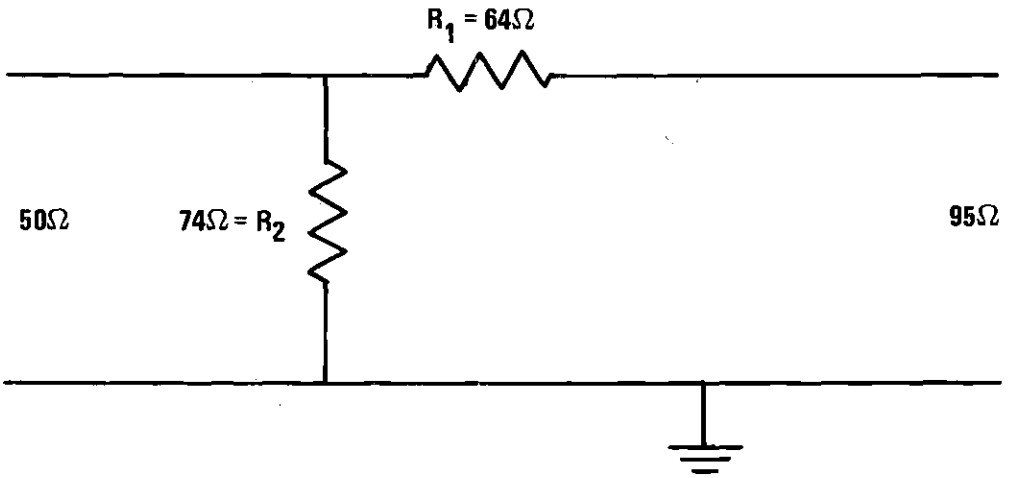

Figure 11. Impedance Matching Network During Calibration

With the initial calibration voltage amplitude and the attenuation reading, one can then calculate the magnitude of the attenuated calibration voltage. Both attenuators had an accuracy of ± 0.05 dB. per 10 dB. increment, while dial readings were recorded in units of 0.02 dB.

To minimize the possibility of error in changing scales on the boxcar integrator, both pulse height and scale were always recorded as a pair. During the calibration procedure, a particular pulse height was always matched to the same scale on which it was originally recorded.

CHAPTER V

RESULTS AND CONCLUSIONS

Amplitude Measurements

A sample of the results of the experiments on three different sodium chloride single crystals using the capacitance microphone detector is shown in Table 7 in Appendix B. In Figure 12 the results of Table 7 are depicted and demonstrate the quadratic dependence of the second harmonic amplitude on the fundamental amplitude in various crystalline orientations using the capacitance microphone detector. Figures 13 - 16 are graphical representations of the data shown in Table 8 in Appendix B. These data verify the quadratic dependence of the second harmonic amplitude on the fundamental amplitude using the magnetic detector. Figures 13 and 14 depict this dependence for longitudinal waves, while Figures 15 and 16 demonstrate this dependence for transverse waves. The quadratic dependence of A_2 on A_1 is a critical experimental test of the theory [see Equation (40)] which permits measurement of third-order elastic constants by the techniques employed in these studies.

The non-linearity parameters K_3, which appear in Equation (33) and which are composed of third-order elastic constants, have been computed from the data obtained using five separate measurement procedures on four different single crystals of NaCl. The determination of K_3 depends on two other parameters, b and K_2, a constant and a combination of second-order elastic constants respectively. K_2 and b are related

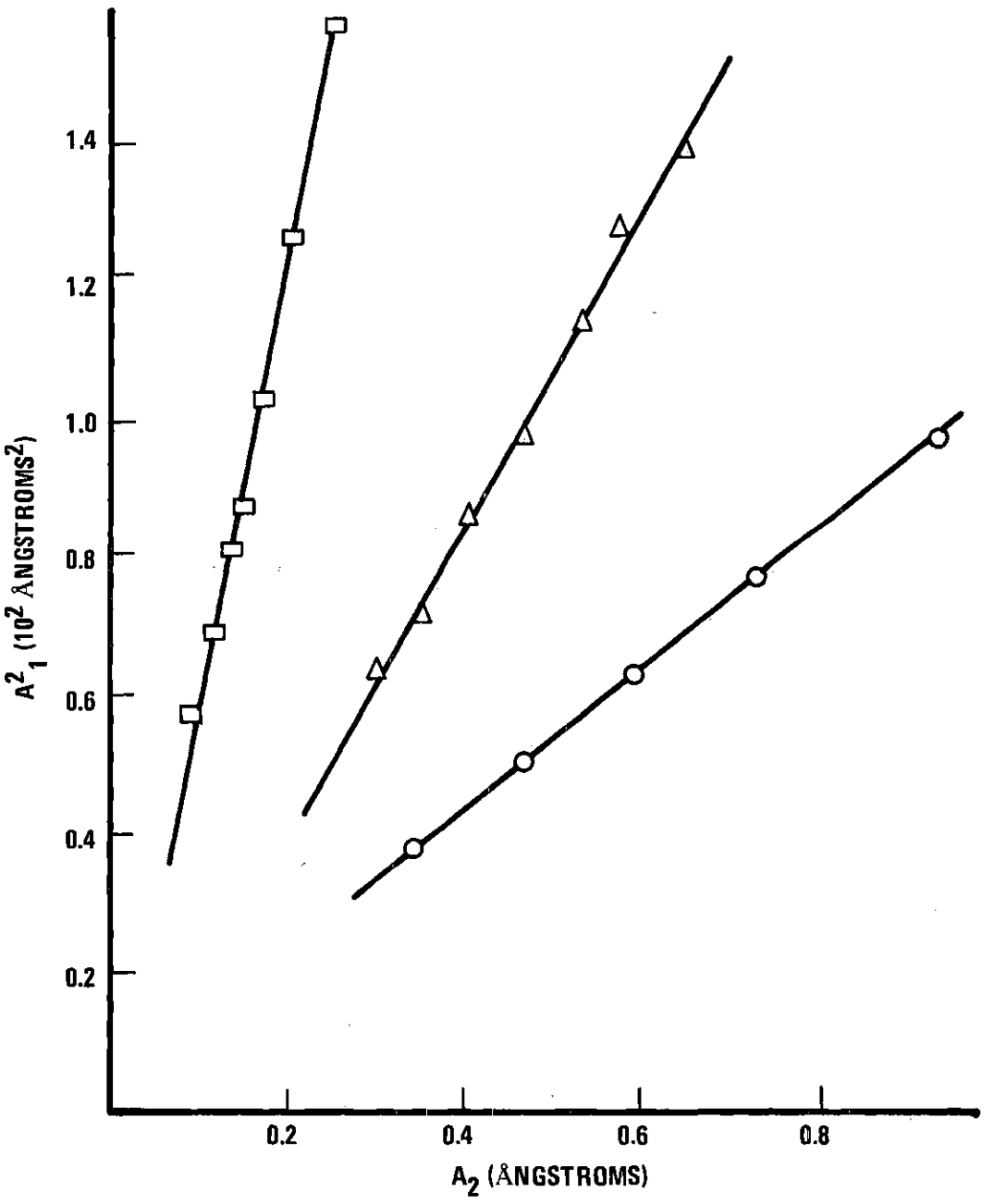

Figure 12. The Quadratic Dependence of the Second Harmonic Amplitude on the Fundamental Amplitude (Capacitance Microphone Detector, Longitudinal Waves Propagating in the [100], [110], or [111] Direction)

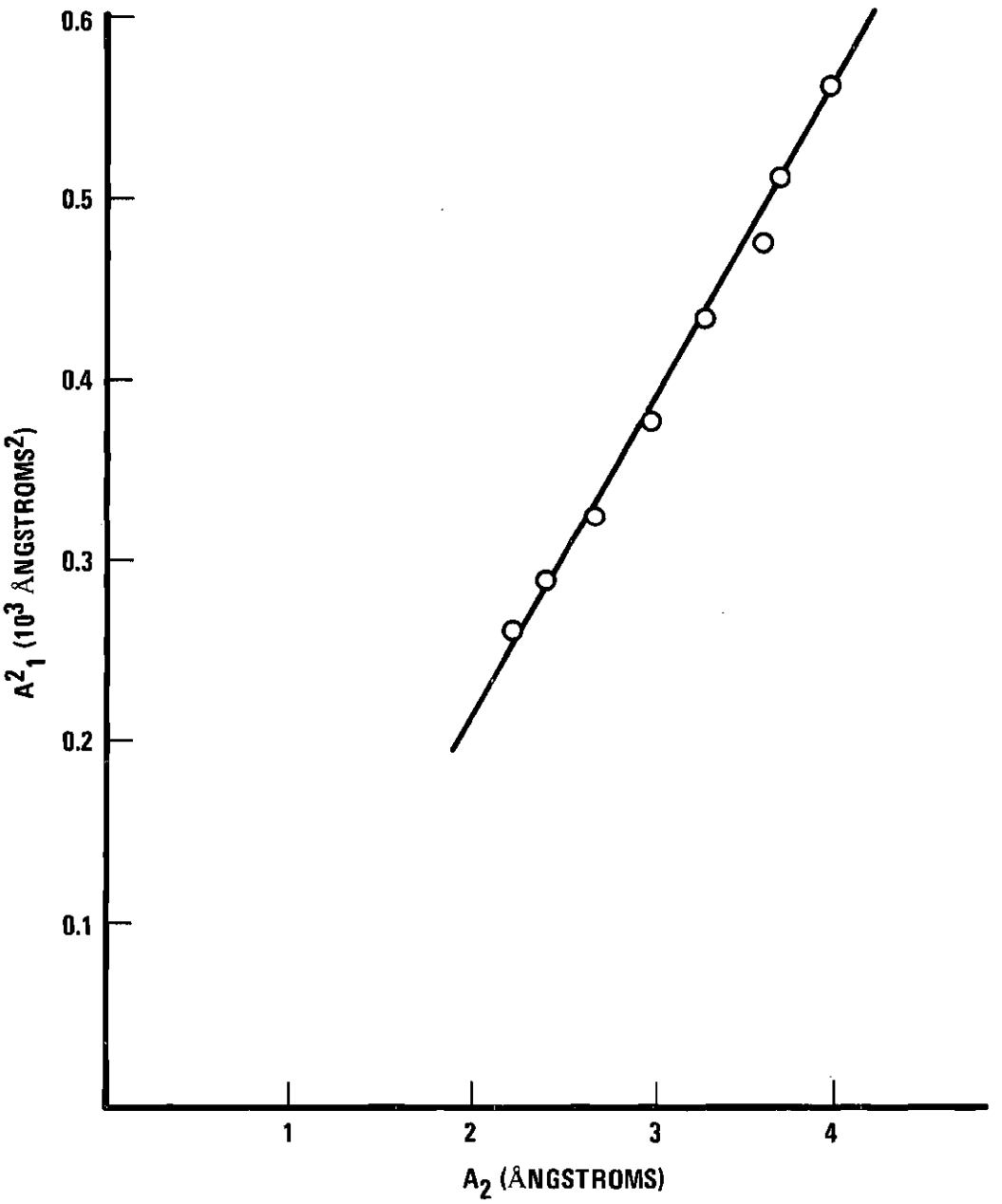

Figure 13. The Quadratic Dependence of the Second Harmonic Amplitude on the Fundamental Amplitude (Magnetic Detector, Longitudinal Waves Propagating in the [100] Direction)

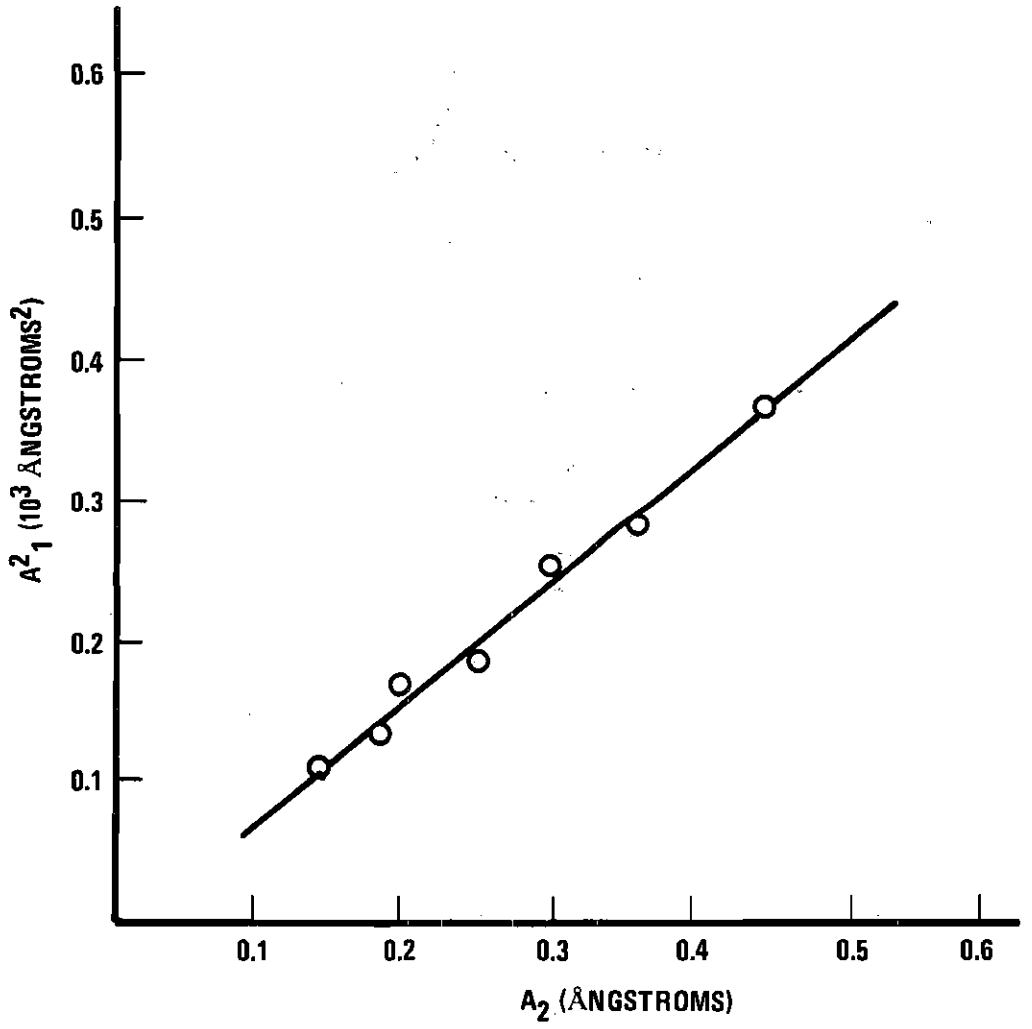

Figure 14. The Quadratic Dependence of the Second Harmonic Amplitude on the Fundamental Amplitude (Magnetic Detector, Longitudinal Waves Propagating in the [111] Direction)

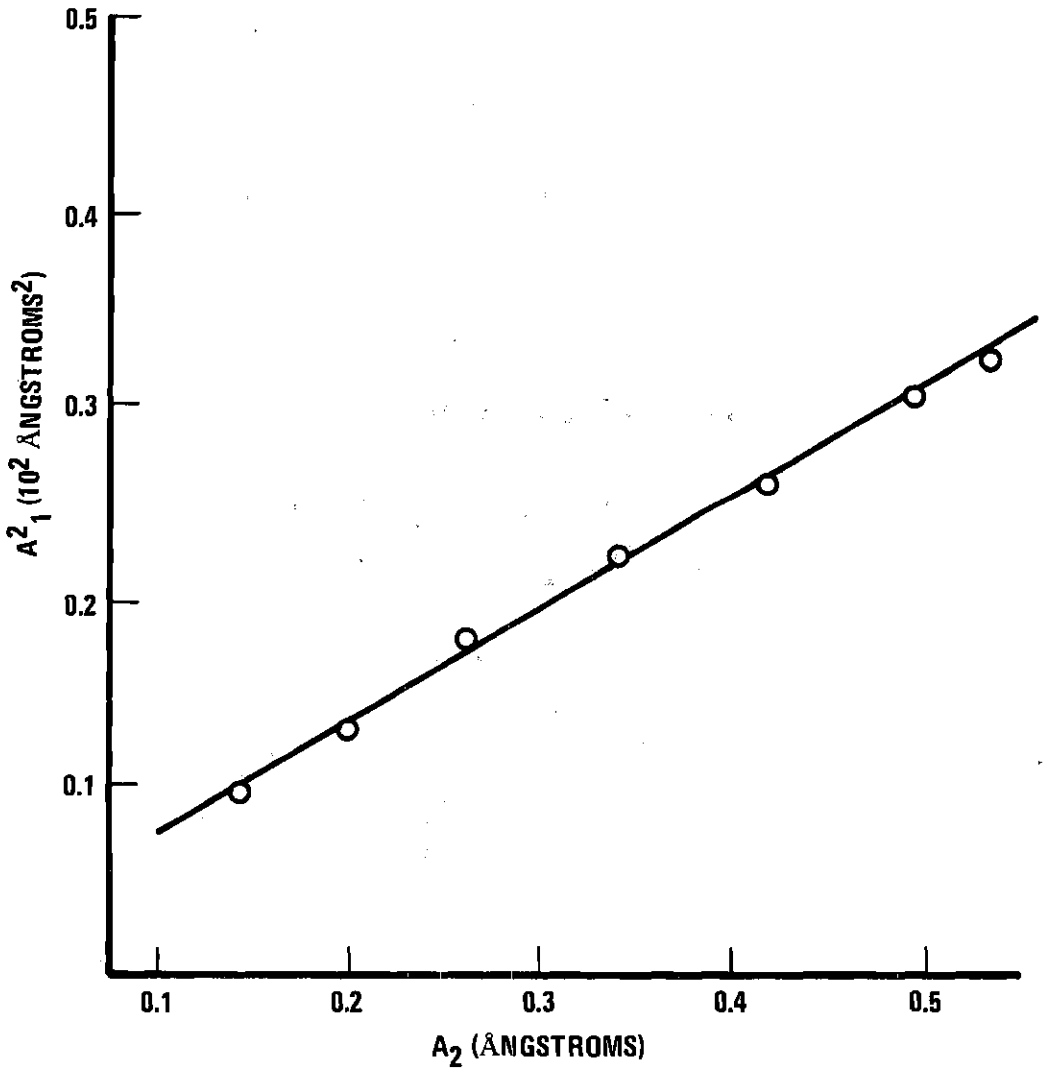

Figure 15. The Quadratic Dependence of the Second Harmonic Amplitude on the Fundamental Amplitude (Magnetic Detector, Transverse Waves Oriented in [$\bar{2}$11] Direction Propagating in [111] Direction

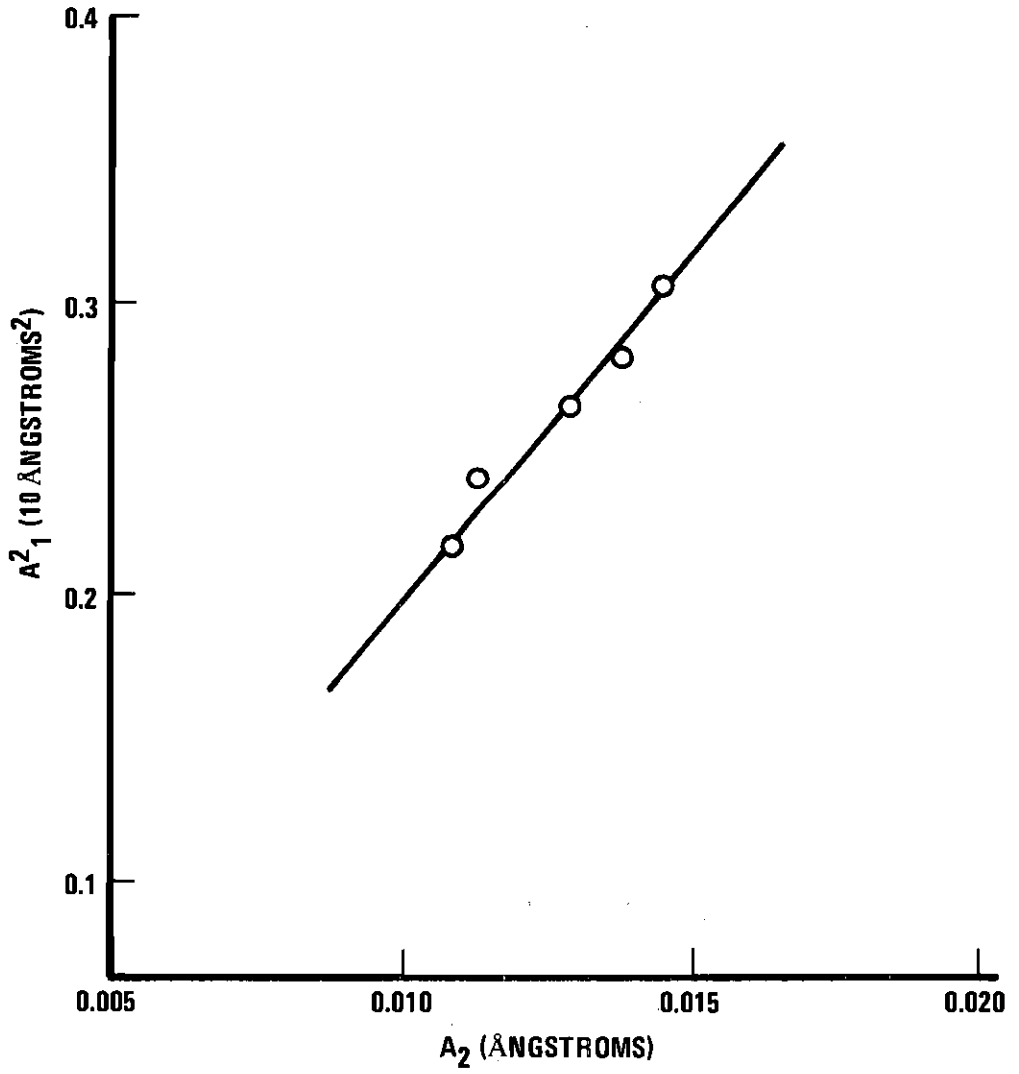

Figure 16. The Quadratic Dependence of the Second Harmonic Amplitude on the Fundamental Amplitude (Magnetic Detector, Transverse Waves Oriented in [$\bar{1}\bar{1}$5] Direction Propagating in [221] Direction

to the coefficient ν in the equation of motion, Equation (32), by the relation $\nu = K_3 + bK_2$. In evaluating K_3, the second-order elastic constants used were those given by Holt (39):

$$C_{11} = 0.487 \qquad C_{12} = 0.124 \qquad C_{44} = 0.126$$

in units of 10^{12} dynes/cm.^{2}

The values of K_3 computed from the various experimental arrangements of propagation and polarization directions are tabulated in Table 3. The root-mean-square error of each measurement procedure is a measure of its precision, and these values are also tabulated for each experimental arrangement in Table 3.

The third-order elastic constants are not a function of sample dimensions, and this independence has been verified in similar experiments using capacitance microphone techniques by Gauster (63). All crystals used in this work were 3.8 cm. in length and 2.5 cm. in diameter, regardless of orientation with respect to crystalline directions.

Calculation of Third-order Elastic Constants

The non-linearity parameters K_3 obtained in these experiments are the values of those linear combinations of third-order elastic constants listed in Table 2 in Chapter II. To determine the entire set of six elastic constants, it is necessary to obtain a sixth relationship among the C's. One might use for this relationship a value of some combination of C's obtained from either hydrostatic pressure or uniaxial stress experiments. Still another, and perhaps preferable, method of obtaining a sixth relationship is to consider the results of theoretical predictions for third-order elastic constants.

Table 3. The Non-linearity Parameters of Sodium Chloride

Propagation Direction	Polarization Direction	K_3 (10^{12} dyne/cm.^{2})	RMS Error (10^{12} dyne/cm.^{2})
[100]	[100]	-9.5	± 1.2
[110]	[110]	-5.5	± 0.5
[111]	[111]	-3.0	± 0.5
[111]	[$\bar{2}$11]	+0.21	± 0.04
[221]	[$\bar{1}\bar{1}$5]	-0.54	± 0.11

Birch (11) has pointed out that for NaCl-type structures using a central force model at absolute zero, the following so-called Cauchy relations are found:

$$C^{O}_{112} = C^{O}_{166} \quad \text{and} \quad C^{O}_{123} = C^{O}_{144} = C^{O}_{456}, \tag{70}$$

where the zero superscript denotes 0°K. Both Nran'yan (52) and Ghate (15) have shown that for NaCl at finite temperatures the relationship

$$C_{144}(T) = C_{456}(T) \tag{71}$$

is still quite good, although the remaining Cauchy relations no longer are valid.

With the acceptance of Equation (71) as a sixth linear relationship, the system of equations represented by Table 2 may now be solved explicitly for each of the third-order elastic constants by standard matrix methods. Table 4 shows the resulting values determined for the third-order elastic constants for NaCl, along with both theoretical calculations and other experimentally determined values of previous investigators.

Discussion of Results

In comparing the present data with previously published theoretical and experimental data for sodium chloride, one notes that there are wide variations in the reported values of the third-order elastic constants. The largest discrepancy between the present data and the others is in the value of C_{123}. The Cauchy condition $C_{112} =$

Table 4. The Third-order Elastic Constants of Sodium Chloride at 300°K

Investigator	Year and Type of Study	C_{111}	C_{112}	C_{144}	C_{166}	C_{123}	C_{456}
		(in units of 10^{12} dynes/cm.^{2})					
Trebits	1971 exper.	-9.5	-0.79	+0.19	-0.83	+0.90	+0.19
Bross	1963 theor.	-13.07	-0.47	+0.26	-0.47	+0.26	+0.26
Nran'yan	1963 theor.	-5.45	-0.69	+0.35	-0.63	+0.27	+0.36
Ghate	1965 theor.	-8.61	-0.52	+0.26	-0.57	+0.16	+0.25
Lincoln et al.	1966 theor.	-8.20	-0.64	+0.25	-0.64	+0.25	+0.25
Paul	1970 theor.	-8.97	-0.70	+0.27	-0.86	+0.15	+0.27
Parker, et al.	1964 exper.	-6.42					
Chang	1965 exper.	-8.80	-0.571	+0.257	-0.611	+0.284	+0.271
Swartz	1966 exper.	-8.64	-0.50	+0.07	-0.59	+0.09	+0.13
Stanford, Zehner	1966 exper.	-8.30					
Gluyas	1967 exper.	-8.23	+0.02	+0.23	-0.61	+0.53	+0.20
Drabble, Strathen	1967 exper.	-8.43	-0.50	+0.29	-0.60	+0.46	+0.26

C_{166} appears to be fulfilled, contrary to theoretical predictions. However, the predicted inequality of C_{123} and C_{144} appears to be borne out.

The effects of error propagation in determining the set of elastic constants is alarmingly significant. If the experimentally determined value for K_3 for each of the propagation and polarization direction pairs is arbitrarily changed by ten per cent (larger, in the absolute sense), the set of elastic constants is calculated to be

$$C_{111} = -10.4 \qquad C_{166} = -0.27$$

$$C_{112} = -3.65 \qquad C_{123} = -2.44$$

$$C_{144} = +0.54 \qquad C_{456} = +0.54$$

in units of 10^{12} dynes/cm.^{2} The values of C_{112} and C_{123} are seen to be particularly sensitive to changes in values of the K_3's, while C_{144} and C_{166} are much less affected.

This sensitivity clearly demonstrates the importance of error propagation in the evaluation of the elastic constants. Two possible sources of error are those of crystal purity and crystal orientation.

Hart (65) measured the second-order elastic constants of several alkali halides in an effort to remove the many discrepancies in published values for those constants, many of which were too large to be accounted for by individual experimental error. In measuring these constants in samples taken from the same parent crystal by three different experimental techniques, he obtained close agreement among the data and concluded that previous discrepancies might be due to differences in the single crystals used by the different experimenters. In measuring C_{111} of NaCl, Parker, Kelly, and Bolef (33) also found that the two

crystals used, obtained from different sources, showed appreciable differencies in elastic constant behavior. Hikata, Chick, Elbaum, and Truell (66) noted experimental evidence of a dislocation contribution to the second harmonic generation of ultrasonic waves in a sample. Thus, the annealing process used becomes extremely important in minimizing this effect.

In the present experiments one sample was cut with its cylindrical axis along the [221] crystallographic direction and its ends perpendicular to this direction. This selection of propagation direction is, at best, a close approximation to that direction specified by Holt (39) for the corresponding combination of third-order elastic constants given in Table 2: the [0.672, 0.672, 0.311] direction. The specified polarization direction [-0.192, -0.192, 0.963] was also approximated by [$\bar{1}\bar{1}5$] during alignment for transverse mode operation. However, the magnitudes of the errors introduced by this selection of directions amount to only 1.2 degrees in the propagation direction and to only 1.9 degrees in the polarization direction.

The principal sources of measurement error in the use of the capacitance mircrophone detector lie in the measurement of the gap capacitance and in the calibration of the detector and amplifier system. Because the gap capacitances were very small, on the order of 30 pf., an uncertainty of even a single picofarad results in a relatively large percentage error. Another possible source of error was the lack of precise frequency control of the pulsed oscillator. A tabulation of possible experimental error in individual parameters is shown in Table 5. Reasonable estimates of the total experimental error can then be

Table 5. Possible Experimental Error in Individual Parameters

Parameter	Magnitude of Error/Typical Value	Per Cent Error
L	estimated	2.0
V_{s1}	0.01/1.00 volts	1.0
V_{s2}	0.01/1.00 volts	1.0
J	estimated	3.0
C	1/25 picofarads	4.0
V_1	0.1/10.0 volts	1.0
V_2	1/100 volts	1.0
Y_1	0.02/60 decibels	0.025
Y_2	0.02/60 decibels	0.025
F	estimated	0.5
F_2	estimated	1.0
T	0.1/10.0 microseconds	1.0
B	estimated	5.0
ℓ	0.04/1.00 centimeters	4.0

made in the determination of the non-linearity parameters K_3, as tabulated in Table 6.

While the problem of accurate determination of gap capacitance does not, of course, arise when using the magnetic detection technique, the problem of precise frequency control remains. In addition, there is some uncertainty in the magnitude of the magnetic field strength and in the length of the evaporated gold strip in the detector. Total experimental errors in the determination of K_3 using the magnetic detector are also depicted in Table 6.

Equation (61) describes a non-linearity parameter K_3 in terms of the appropriate combination K_2 of second-order elastic constants and various measured parameters. The displacement amplitude of the ith harmonic A_i in Equation (61), using the capacitance microphone technique, is determined by the expression

$$A_i = \frac{V_{si} \cdot 10^{-Y_i/20}}{JCV_i} , \tag{72}$$

where V_i is the capacitance microphone bias voltage, Y_i is the calibration attenuation in decibels, $J = 1/\epsilon W$ is the reciprocal of the product of the permitivity of air ϵ and the detector button area W, C is the capacitance of the sample-button capacitor, and V_{si} is the calibration voltage (see Chapter IV). Inserting Equation (72) into Equation (61) yields

$$K_3 = - bK_2 - \frac{4LV_{s2}JCV_1^2K_2 \cdot 10^{Y_1/10-Y_2/20}}{(\pi FTV_{s1})^2V_2} , \tag{73}$$

Table 6. Estimated Percentage Errors of the Non-linearity Parameters of Sodium Chloride

Propagation	Polarization	K_3 (10^{12} dynes/cm.^{2})	Capacitance Microphone Estimated Error (Per cent)		Magnetic Detector Estimated Error (Per cent)	
[100]	[100]	-9.5	± 1.6	17.0	± 1.4	14.7
[110]	[110]	-9.5	± 0.8	15.3	-	-
[111]	[111]	-3.0	± 0.4	11.7	± 0.3	10.2
[111]	[$\bar{2}$11]	+0.21	-	-	± 0.05	22.4
[221]	[$\bar{1}\bar{1}$5]	-0.54	-	-	± 0.12	21.7

where an extra factor of two appears in the second term due to the fact that the crystal receiving end is a stress-free boundary.

The expression corresponding to Equation (72) for the magnetic detection technique is given by Equation (67). In terms of experimentally measured quantities, the displacement amplitude of the ith harmonic A_i in Equation (67) is given by

$$A_i = \frac{V_{si} \cdot 10^{-Y_i/20}}{4\pi F_i B \ell} , \tag{74}$$

where B is the magnetic field strength, ℓ is the length of the gold strip evaporated onto the sample face, and F_i is the frequency of the ith harmonic. Insertion of Equation (74) into Equation (61) then yields

$$K_3 = - bK_2 - \frac{16LB\ell V_{s2}K_2 \cdot 10^{Y_1/10-Y_2/20}}{\pi F_2 (V_{s1}T)^2} . \tag{75}$$

Again the extra factor of two has been taken into account.

Table 5 lists the experimentally determined parameters found in Equations (73) and (75) with in indication of the accuracy obtainable for the measurement of each parameter and the corresponding possible percentage error. With the capacitance microphone technique, a possible experimental error of up to 17.0 per cent results for the calculated values of the non-linearity parameters K_3. With the magnetic detection technique, the possible experimental error in K_3 is determined to be up to 14.7 per cent for longitudinal waves propagating in crystals whose axes were oriented in the [100] or [111] direction. Possible

errors of up to 22.4 per cent result for the crystals whose axes were oriented in the [111] or [221] direction, and where the transverse orientation of the AC-cut transducer requires an additional five per cent error estimate.

Recommendations

Table 4, which records the history of both theoretical and experimental studies of third-order elastic constants for NaCl, has two obvious features. First, there is a wide variance among reported experimental values determined using a variety of measurement techniques. Second, one may observe a discernible, though not surprising, discrepancy between experiment and theory.

Parker, Kelly, and Bolef (33) have already noted an inexplicable variation in the elastic parameters of individual crystals of NaCl obtained from different sources. Whether or not this is the major reason for the wide variance in measured values of third-order elastic constants could be determined by using one or two single crystals. Each crystal would have to be studied serially by those different laboratories having the specialized facilities appropriate to each of the different measurement techniques.

The magnetic detection technique described in the present work offers a means of checking measurements by uniaxial stress and hydrostatic pressure techniques. This technique permits the measurement of transverse acoustic wave amplitudes, a feature of elastic measurement not heretofore utilized.

APPENDICES

APPENDIX A

RESPONSE OF THE EQUIVALENT DETECTOR CIRCUIT TO SAMPLE DISPLACEMENTS

Equation (63) may be derived from a consideration of the equivalent electrical circuit shown in Figure 3. This circuit is redrawn with its relevant electrical parameters as shown in Figure 17. The current i_1 flows about loop C, V_0, R_1, and the current i_2 flows about loop C, C_2, R_2. The following notation will be used:

C = instantaneous gap capacitance,

C_0 = quiescent gap capacitance,

s = instantaneous gap width,

s_0 = quiescent gap width.

The last two parameters are related by the equation

$$s = s_0 + \Delta s \sin \omega t, \tag{76}$$

where

Δs = vibration amplitude of the sample,

ω = angular frequency of vibration,

t = time.

V_0, R_1, R_2, and C_2 are depicted in Figure 17. Since the structure

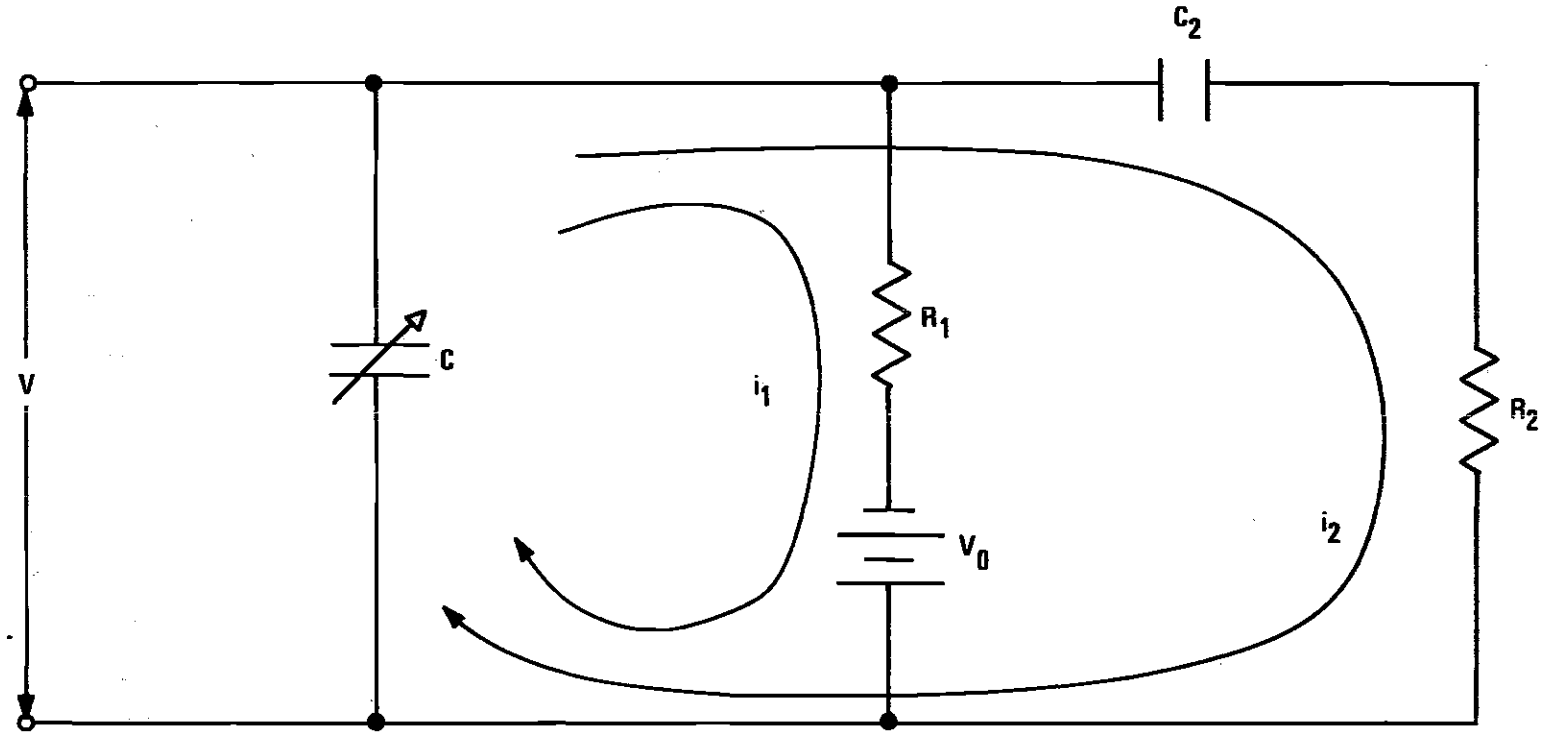

Figure 17. Input Equivalent Circuit of the Capacitance Microphone Detector and Preamplifier

formed by the detector button and sample end face represents a parallel plate capacitor, we may write

$$C_0 = \frac{\epsilon W}{s_0} , \tag{77}$$

where $\epsilon = 8.86 \times 10^{-12}$ in M. K. S. units, and W is the area of the center button in meters^2. The instantaneous gap capacitance will then be

$$C = \frac{\epsilon W}{s} . \tag{78}$$

With the substitution of Equation (76) for s, Equation (78) becomes

$$\frac{1}{C} = \frac{s}{\epsilon W} = \frac{s_0}{\epsilon W}(1 + \frac{\Delta s}{s_0} \sin \omega t), \tag{79}$$

or

$$\frac{1}{C} = \frac{1}{C_0} [1 + \gamma \sin \omega t] , \tag{80}$$

where $\gamma = \frac{\Delta s}{s_0}$ as in Chapter III.

If Q_1 and Q_2 are the charges on capacitors C and C_2 respectively, then the two loop equations are given by

$$R_1 \frac{dQ_1}{dt} + \frac{1}{C}[Q_1 + Q_2] = V_0 \tag{81}$$

and

$$R_2 \frac{dQ_2}{dt} + \frac{Q_2}{C_2} + \frac{1}{C}[Q_1 + Q_2] = 0 . \tag{82}$$

The desired result is the time-varying voltage output of the detector

$$V = R_1 \frac{dQ_1}{dt} . \tag{83}$$

With the insertion of the expression for 1/C from Equation (80) into Equations (81) and (82), the loop equations become

$$R_1 \frac{dQ_1}{dt} + \frac{1}{C_0}[Q_1 + Q_2][1 + \gamma \sin \omega t] = V_0 \tag{84}$$

and

$$R_2 \frac{dQ_2}{dt} + \frac{Q_2}{C_2} + \frac{1}{C_0}[Q_1 + Q_2][1 + \gamma \sin \omega t] = 0. \tag{85}$$

If Equation (84) is solved for Q_2 and then differentiated with respect to time, the variables Q_2 and $\frac{dQ_2}{dt}$ can be eliminated from Equation (85). One then seeks a solution to the resulting second-order differential equation with variables Q_1 and $\frac{dQ_1}{dt}$:

$$[-R_1R_2C_0] \frac{d^2Q_1}{dt^2} + R_1[R_2C_0\gamma\omega \cos \omega t - (1 + \frac{R_2}{R_1}) \gamma \sin \omega t \tag{86}$$

$$- (1 + \frac{R_2}{R_1} + \frac{C_0}{C_2})] \frac{dQ_1}{dt} - \frac{1}{C_2}[1 + \gamma \sin \omega t] Q_1$$

$$+ V_0[1 + \frac{C_0}{C_2} + \gamma \sin \omega t - R_2C_0 \gamma\omega \cos \omega t] = 0.$$

We now assume a Fourier series solution to Equation (86) for Q_1:

$$Q_1 = \sum_{n=0}^{\infty} (a_n \sin n\omega t + b_n \cos n\omega t). \tag{87}$$

This expression for Q_1 is substituted into Equation (86), where one

retains only the n = 0 and n = 1 terms. The resulting equation is

$$[(R_1R_2C_0\omega^2 - \frac{1}{C_2})a_1 + \omega R_1(1 + \frac{C_0}{C_2} + \frac{R_2}{R_1})b_1 - \frac{\gamma}{C_2} b_0 + \gamma V_0]\sin \omega t \qquad (88)$$

$$+ [-\omega R_1(1 + \frac{C_0}{C_2} + \frac{R_2}{R_1})a_1 + (R_1R_2C_0\omega^2 - \frac{1}{C_2})b_1 - R_2C_0 \gamma\omega V_0]\cos \omega t$$

$$+ [\frac{\gamma}{2}(R_1R_2C_0\omega^2 - \frac{1}{C_2})a_1 + \frac{1}{2}R_1\gamma\omega(1 + \frac{R_2}{R_1})b_1 - \frac{b_0}{C_2} + V_0(1 + \frac{C_0}{C_2})]$$

$$+ [\text{second harmonics}] = 0.$$

Since Equation (88) must be valid for all times t, we may equate separately the coefficient of each sine, cosine, and constant term to zero. The resulting three equations in the three unknowns a_1, b_0, and b_1 may then be solved for the desired quantities a_1 and b_1. Since the time-varying output voltage will be just

$$V = R_1 \frac{dQ_1}{dt} = R_1[a_1\omega \cos \omega t - b_1\omega \sin \omega t], \qquad (89)$$

the coefficient b_0 of the constant term in Equation (87) need not be calculated.

After a great deal of time-consuming arithmetic, one finds that the time-varying component of the output voltage of the capacitance microphone detector capacitively connected to a preamplifier of given input impedance is given by

$$V = \frac{\gamma V_0 R_2 C_0 \omega \left[1 + \left(\frac{C_0}{C_2}\right)^2 (R_2 C_0 \omega)^{-2}\right]^{1/2}}{\left[\left(1 + \frac{C_0}{C_2} + \frac{R_2}{R_1}\right)^2 + \left(R_2 C_0 \omega - \frac{1}{\omega R_1 C_2}\right)^2\right]^{1/2}} \quad . \tag{90}$$

For F = 30 MHz, C_0 = 25 pf., C_0/C_2 = 0.05, R_2/R_1 = 0.04, R_2C = 180 radians, and RC = 9×10^4 radians, this output voltage is just γV_0 to an error of 0.5 per cent.

Since the measurement of importance in this experiment is the amplitude of the second harmonic ultrasonic signal generated within the sample crystal, it is absolutely essential that any second harmonic signal generated by the detector itself be much smaller in magnitude than the crystal generated signal. To determine whether or not this particular detector fulfills this requirement, one can extend the analysis of the previous discussion by considering the effects of including the n = 2 terms in the Fourier solution of Equation (86). When this is done, it is found that the ratio of the second harmonic voltage amplitude V_2 to the fundamental voltage amplitude V_1 is given by

$$\left|\frac{V_2}{V_1}\right| = \frac{2\gamma\left[(R_0 C_2 \omega)^2 + \left(\gamma \frac{C_0}{C_2}\right)^2\right]^{1/2}}{\left[\left(\frac{1}{R_1 C_2 \omega} - 4R_2 C_0 \omega\right)^2 + 4\left(1 + \frac{C_0}{C_2} + \frac{R_2}{R_1}\right)^2\right]^{1/2}} \quad . \tag{91}$$

Since γ is on the order of 10^{-4}, this voltage ratio is approximately equal to

$$|V_2/V_1| \approx \frac{1}{2}\gamma = 0.5 \times 10^{-4} \quad , \tag{92}$$

with the same parameters as before. Thus, the second harmonic produced

by the detector itself is at least 80 dB. below the fundamental amplitude. But since the second harmonic generated within the sample is only 40 dB. below the fundamental amplitude, it is still some 40 dB. above the second harmonic produced by the detector.

Experimental verification of this conclusion was determined by injecting an attenuated 30 MHz signal into the auxiliary detector input jack and decreasing the amount of attenuation until an observable amount of 60 MHz output signal was produced. The results of this procedure bore out the validity of the above estimates.

APPENDIX B

Sample: NaCl[100] Polarization: [100] Date: 10 Sept. 1970

PHV	CH	SCL	VOLT	ATTEN dB.	A_1 10^{-7} cm.	A_1^2 10^{-14} cm.^{2}	A_2 10^{-8} cm.	K_3 10^{12} dyn/cm.^{2}
75	1	20	6.73	70.35	0.759	0.576	0.527	-10.1
	2	20	95.2	70.50				
70	1	20	7.07	70.35	0.723	0.522	0.478	-10.1
	2	20	105	70.50				
65	1	20	7.59	70.35	0.673	0.453	0.420	-10.0
	2	20	122	70.50				
60	1	20	8.10	70.35	0.631	0.398	0.364	-10.1
	2	20	138	70.50				
55	1	20	8.59	70.35	0.595	0.354	0.320	-10.0
	2	20	157	70.50				
50	1	20	9.40	70.35	0.544	0.295	0.270	-10.1
	2	20	186	70.50				
45	1	20	10.1	70.35	0.506	0.256	0.230	- 9.90
	2	20	218	70.50				
40	1	20	11.2	70.35	0.456	0.208	0.200	-11.9
	2	20	274	70.50				
35	1	20	12.5	70.35	0.409	0.167	0.146	- 9.80
	2	20	338	70.50				

Fund. Freq. = 27.0 D.M. = 29.3 MHz
Sec. Harm. = 57.6 C.M. = 58.6 MHz

Capacitance with Crystal = 160 pf.
Capacitance w/o Crystal = 135 pf.
Net Gap Capacitance = 25 pf.

X1 = 10 X2 = 2.5

V_s = 0.5 volts
J = 11.89
C = 25 pf.
a = 3.8 cm.
L = 2.6 cm.
F = 29.3 MHz
T = 8.0 μ sec
K_2 = 0.49 x 10^{12} dynes/cm.^{2}

Figure 18. Sample Data Sheet Using the Capacitance Microphone Detector

Sample: NaCl[111] Polarization: [$\bar{2}$11] Date: 11 May 1971

PHV	CH	SIG	SCL	I	B wb/m^2	ATTEN. dB.	A_1 10^{-7}cm.	A_1^2 10^{-14}cm.^{2}	A_2 10^{-9}cm.	K_3 10^{12}dyn/cm.^{2}
47	1	10	20	1.83	.120	65.6	0.565	0.319	0.532	+0.229
	2	1.85	2.0	10	.468	94.3				
45	1	10	20	1.88	.124	65.6	0.547	0.299	0.491	+0.226
	2	1.65	2.0	10	.468	95.0				
43	1	10	20	1.99	.129	65.6	0.526	0.276	0.469	+0.234
	2	1.50	2.0	10	.468	95.4				
41	1	10	20	2.09	.135	65.6	0.502	0.252	0.418	+0.228
	2	1.25	2.0	10	.468	96.4				
39	1	10	20	2.20	.142	65.6	0.477	0.228	0.360	+0.217
	2	0.95	2.0	10	.468	97.7				
37	1	10	20	2.30	.147	65.6	0.461	0.213	0.336	+0.217
	2	0.82	1.0	10	.468	98.3				
35	1	10	20	2.52	.161	65.6	0.421	0.177	0.296	+0.230
	2	0.68	1.0	10	.468	99.4				
33	1	10	20	2.61	.166	65.6	0.408	0.167	0.264	+0.218
	2	0.55	1.0	10	.468	100.4				
31	1	10	20	2.93	.185	65.6	0.367	0.134	0.232	+0.238
	2	0.39	0.5	10	.468	101.5				

Fund. Freq. = 29.5 D.M. = 29.9 MHz
Sec. Harm. = 61.3 D.M. = 59.8 MHz

X1 = 10 X2 = 4.5

V_s = 0.5 volts
F_ℓ = 29.9 MHz
ℓ = 1.03 cm.
T = 12.9 μsec.
a = 3.8 cm.
L = 3.1 cm.
$K_2 = 0.163 \times 10^{12}$ dynes/cm.^{2}

Figure 19. Sample Data Sheet Using the Magnetic Detector

Table 7. Amplitude Measurements in Sodium Chloride Using the Capacitance Microphone Detector

Propagation Direction	Polarization Direction	Fundamental Amplitude A_1 (Ångstroms)	Second Harmonic Amplitude A_2 (Ångstroms)	A_2/A_1^2 (10^{-3} Ångstroms^{-1})
[100]	[100]	12.6	1.13	7.12
		11.6	0.946	7.06
		10.4	0.758	7.03
		9.25	0.599	7.02
		8.34	0.491	7.06
		9.74	0.875	9.23
		9.34	0.795	9.11
		8.88	0.710	9.02
		8.21	0.597	8.85
		7.66	0.523	8.93
		6.94	0.425	8.83
		6.30	0.352	8.89
		5.57	0.276	8.88
		4.86	0.206	8.74
		8.85	0.673	8.58
		8.13	0.585	8.87
		7.05	0.437	8.78
		6.42	0.366	8.87
		5.35	0.251	8.78
		10.8	1.12	9.57
		9.75	0.923	9.71
		8.66	0.721	9.60
		7.79	0.583	9.60
		7.06	0.462	9.26
		6.09	0.338	9.11
[110]	[110]	11.62	0.644	4.77
		11.12	0.570	4.62
		10.59	0.529	4.73
		9.83	0.468	4.85
		9.19	0.402	4.76
		8.40	0.349	4.95
		7.84	0.304	4.94

Table 7. Amplitude Measurements in Sodium Chloride Using the Capacitance Microphone Detector (continued)

Propagation Direction	Polarization Direction	Fundamental Amplitude A_1 (Ångstroms)	Second Harmonic Amplitude A_2 (Ångstroms)	A_2/A_1^2 (10^{-3} Ångstroms^{-1})
[110]	[110]	12.7	0.773	4.77
		11.6	0.655	4.89
		10.7	0.563	4.90
		9.91	0.481	4.90
		9.00	0.387	4.79
		8.12	0.318	4.82
		14.5	0.917	4.39
		13.1	0.758	4.40
		12.1	0.648	4.44
		11.1	0.549	4.43
		10.0	0.451	4.46
		9.47	0.400	4.46
		8.43	0.321	4.52
		10.24	0.547	5.21
		9.57	0.485	5.29
		8.93	0.428	5.37
		8.37	0.367	5.24
		7.65	0.310	5.31
		7.05	0.263	5.31
		6.24	0.213	5.46
[111]	[111]	11.91	0.241	1.70
		11.35	0.219	1.70
		10.70	0.194	1.69
		9.95	0.169	1.71
		9.07	0.139	1.69
		13.67	0.314	1.68
		12.43	0.260	1.68
		11.13	0.211	1.70
		10.26	0.176	1.67
		9.27	0.156	1.84
		8.97	0.139	1.73
		8.26	0.118	1.73
		7.53	0.097	1.71

Table 7. Amplitude Measurements in Sodium Chloride Using the Capacitance Microphone Detector (continued)

Propagation Direction	Polarization Direction	Fundamental Amplitude A_1 (Ångstroms)	Second Harmonic Amplitude A_2 (Ångstroms)	A_2/A_1^2 (10^{-3} Ångstroms^{-1})
[111]	[111]	8.62	0.155	2.09
		8.11	0.138	2.10
		7.52	0.119	2.10
		6.89	0.101	2.13
		6.46	0.088	2.11
		6.07	0.081	2.20
		11.86	0.298	2.12
		11.50	0.279	2.11
		10.79	0.243	2.09
		10.42	0.222	2.05
		9.79	0.198	2.07
		9.14	0.170	2.04
		8.59	0.148	2.01
		8.18	0.134	2.01
		7.50	0.114	2.03
		7.01	0.097	1.98

Table 8. Amplitude Measurements in Sodium Chloride Using the Magnetic Detector

Propagation Direction	Polarization Direction	Fundamental Amplitude A_1 (Ångstroms)	Second Harmonic Amplitude A_2 (Ångstroms)	A_2/A_1^2 (10^{-3} Ångstroms^{-1})
[100]	[100]	16.6	0.222	8.08
		15.2	0.194	8.36
		13.4	0.174	9.68
		12.0	0.146	10.01
		11.3	0.119	9.38
		9.9	0.100	10.02
		23.6	0.405	7.25
		22.6	0.372	7.28
		21.7	0.362	7.73
		20.8	0.330	7.64
		19.2	0.304	8.20
		17.9	0.270	8.41
		17.0	0.244	8.41
		16.2	0.227	8.60
		12.7	0.141	8.76
		10.4	0.094	8.63
		14.6	0.191	8.97
		16.7	0.257	9.24
[111]	[111]	18.9	0.448	1.25
		16.6	0.360	1.30
		15.7	0.301	1.22
		13.4	0.245	1.37
		12.6	0.191	1.20
		11.2	0.181	1.44
		10.0	0.141	1.41
		23.3	0.430	0.795
		21.5	0.378	0.818
		19.0	0.313	0.868
		17.3	0.276	0.927
		15.0	0.276	1.23
		13.6	0.193	1.05
		13.1	0.179	1.04

Table 8. Amplitude Measurements in Sodium Chloride Using the Magnetic Detector (continued)

Propagation Direction	Polarization Direction	Fundamental Amplitude A_1 (Ångstroms)	Second Harmonic Amplitude A_2 (Ångstroms)	A_2/A_1^2 (10^{-3} Ångstroms^{-1})
[111]	[111]	23.2	0.471	0.875
		22.7	0.442	0.858
		21.4	0.406	0.885
		19.5	0.368	0.964
		18.6	0.348	1.01
		17.7	0.313	1.00
		16.8	0.292	1.02
		15.7	0.260	1.06
		14.9	0.244	1.10
		13.9	0.214	1.10
[111]	[$\bar{2}$11]	5.65	0.0532	1.67
		5.47	0.0491	1.64
		5.26	0.0469	1.70
		5.02	0.0418	1.66
		4.77	0.0360	1.58
		4.61	0.0336	1.58
		4.21	0.0296	1.67
		4.08	0.0264	1.58
		3.67	0.0232	1.73
		3.50	0.0198	1.62
		3.20	0.0166	1.63
		3.00	0.0143	1.59
		6.40	0.0611	1.49
		5.73	0.0520	1.59
		5.22	0.0413	1.51
		4.52	0.0328	1.60
		4.08	0.0258	1.55
		3.53	0.0187	1.50
		3.05	0.0148	1.59
		2.74	0.0121	1.61
		5.59	0.0585	1.87
		4.91	0.0481	1.99
		4.47	0.0369	1.84
		3.93	0.0277	1.79
		3.51	0.0220	1.79
		3.91	0.0277	1.81

Table 8. Amplitude Measurements in Sodium Chloride Using the Magnetic Detector (continued)

Propagation Direction	Polarization Direction	Fundamental Amplitude A_1 (Ångstroms)	Second Harmonic Amplitude A_2 (Angstroms)	A_2/A_1^2 (10^{-3} Ångstroms^{-1})
[111]	[$\bar{2}$11]	4.27	0.0378	2.06
		4.65	0.0487	2.26
		5.02	0.0592	2.35
[221]	[$\bar{1}$15]	1.74	0.0141	4.66
		1.66	0.0136	4.95
		1.62	0.0129	4.93
		1.55	0.0115	4.80
		1.47	0.0107	4.94
		1.93	0.0156	4.20
		1.86	0.0144	4.16
		1.78	0.0136	4.32
		1.66	0.0129	4.60
		1.53	0.0123	5.24

BIBLIOGRAPHY

1. R. Hooke, De Potentia restitutiva (London, 1678).
2. F. W. Sheard, Phil. Mag. 3, 1381 (1958).
3. Y. Hiki, J. F. Thomas, Jr., and A. V. Granato, Phys. Rev. 153, 764 (1967).
4. H. E. Bommel and K. Dransfeld, Phys. Rev. 117, 1245 (1960).
5. W. P. Mason and T. B. Bateman, J. Acoust. Soc. Am. 36, 644 (1964).
6. H. Pfleiderer, Phys. Stat. Sol. 2, 1539 (1962).
7. R. A. Coldwell-Horsfall, Phys. Rev. 129, 22 (1963).
8. A. L. Cauchy, Exercices de mathématique (1827).
9. L. Brillouin, Ann. Phys. 4, 328 (1925).
10. T. D. Murnaghan, Finite Deformation of an Elastic Solid (John Wiley and Sons, Inc., New York, 1951).
11. F. Birch, Phys. Rev. 71, 809 (1947).
12. R. F. S. Hearmon, Acta. Cryst. 6, 331 (1953).
13. R. F. S. Hearmon, Acta. Cryst. 10, 121 (1957).
14. K. Brugger, Phys. Rev. 133, A1611 (1964).
15. P. B. Ghate, Phys. Rev. 139, A1666 (1965).
16. R. C. Lincoln, K. M. Koliwad, and P. B. Ghate, Phys. Stat. Sol. 18, 265 (1966).
17. C. S. G. Cousins, Proc. Phys. Soc. 91, 235 (1967).
18. T. Suzuki, Phys. Rev. 3, 4007 (1971).
19. D. Lazarus, Phys. Rev. 76, 545 (1949).
20. W. B. Daniels and C. S. Smith, Phys. Rev. 111, 713 (1958).
21. H. J. McSkimin and P. Andreatch, Jr., J. Appl. Phys. 34, 651 (1963).
22. Z. P. Chang and G. R. Barsch, Phys. Rev. Letters 19, 1381 (1967).

23. D. S. Hughes and J. L. Kelly, Phys. Rev. 92, 1145 (1953).

24. T. Bateman, W. P. Mason, and H. L. McSkimin, J. Appl. Phys. 32, 928 (1961).

25. H. J. McSkimin and P. Andreatch, Jr., J. Appl. Phys. 35, 3312 (1964).

26. E. H. Bogardus, J. Appl. Phys. 36, 2504 (1965).

27. R. N. Thurston, H. J. McSkimin, and P. Andreatch, Jr., J. Appl. Phys. 37, 267 (1966).

28. Z. P. Chang, Phys. Rev. 140, A1788 (1965).

29. Y. Hiki and A. V. Granato, Phys. Rev. 144, 411 (1966).

30. J. F. Thomas, Jr., Phys. Rev. 175, 955 (1968).

31. B. E. Powell and M. J. Skove, Phys. Rev. 174, 977 (1968).

32. J. Melngailis, A. A. Maradudin, and A. Seeger, Phys. Rev. 131, 1972 (1963).

33. J. H. Parker, E. F. Kelly, and D. I. Bolef, Appl. Phys. Letters 5, 7 (1964).

34. F. R. Rollins, Jr., Appl. Phys. Letters 2, 147 (1963).

35. F. R. Rollins, Jr., L. H. Taylor, and P. H. Todd, Jr., Phys. Rev. 136, A597 (1964).

36. L. H. Taylor and F. R. Rollins, Jr., Phys. Rev. 136, A591 (1964).

37. J. D. Childress and C. G. Hambrick, Phys. Rev. 136, A411 (1964).

38. P. H. Carr, IEEE Transactions on Sonics and Ultrasonics SU-13, 103 (1966).

39. A. C. Holt, Doctoral Thesis, Georgia Institute of Technology (1967).

40. R. W. Dunham and H. B. Huntington, Phys. Rev. 2, 1098 (1970).

41. J. S. Mendousse, J. Acoust. Soc. Am. 25, 51 (1953).

42. A. A. Gedroĭts and V. A. Krasil'nikov, Sov. Phys. JETP 16, 1122 (1963).

43. D. T. Blackstock, J. Acoust. Soc. Am. 39, 1019 (1966).

44. M. A. Breazeale and J. Ford, J. Appl. Phys. 36, 3486 (1965).

45. O. Buck and D. O. Thompson, Mater. Sci. Eng. 1, 117 (1966).

46. A. C. Holt and J. Ford, J. Appl. Phys. 38, 42 (1967).

47. M. A. Breazeale and D. O. Thompson, Appl. Phys. Letters 3, 77 (1963).

48. W. B. Gauster and M. A. Breazeale, Phys. Rev. 168, 655 (1968).

49. R. D. Peters, M. A. Breazeale, and V. K. Paré, Rev. Sci. Instr. 39, 1505 (1968).

50. A. Hikata, B. B. Chick, and C. Elbaum, J. Appl. Phys. 36, 229 (1965).

51. R. D. Peters and R. T. Arnold, J. Appl. Phys. 42, 980 (1971).

52. A. A. Nran'yan, Sov. Phys. Solid State 5, 129 (1963).

53. S. Paul, Ind. J. Pure & Appl. Sci. 8, 307 (1970).

54. S. Paul, Phys. Stat. Sol. 37, K137 (1970).

55. K. D. Swartz, J. Acoust. Soc. Am. 41, 1083 (1967).

56. M. Ghafelehbashi and K. M. Koliwad, J. Appl. Phys. 41, 4010 (1970).

57. J. R. Drabble and R. E. B. Strathen, Proc. Phys. Soc. 92, 1090 (1967).

58. M. Gluyas, Brit. J. Appl. Phys. 18, 913 (1967).

59. A. L. Stanford, Jr. and S. P. Zehner, Phys. Rev. 153, 1025 (1967).

60. I. G. Mikhailov and V. A. Shutilov, Sov. Phys. Acoustics 10, 77 (1964).

61. W. Keck and R. T. Beyer, Phys. Fluids 3, 346 (1960).

62. H. Seki, A. Granato, and R. Truell, J. Acoust. Soc. Am. 28, 230 (1956).

63. W. B. Gauster, Doctoral Thesis, University of Tennessee (1966).

64. P. Kisliuk, J. Appl. Phys. 25, 897 (1954).

65. S. Hart, Brit. J. Appl. Phys. 1, 1277 (1968).

66. A. Hikata, B. B. Chick, C. Elbaum, and R. Truell, Acta Met. 10, 423 (1962).

VITA

Robert Neil Trebits was born in New York, New York on June 21, 1944. He is the son of Max and Ethel Trebits. He began his formal education in the Marietta, Georgia school system and then attended a succession of grammar schools in the DeKalb County, Georgia school system. He attended Cross Keys High School in the county, and in 1961 entered the Georgia Institute of Technology. He received the degree of Bachelor of Science in Physics with honors in 1965. A Master of Science Degree in physics was awarded in 1967.

He was the recipient of a National Science Foundation research grant in 1967 and a traineeship in 1970. During his several years in graduate school, he was a teaching assistant, instructing classes in sophomore physics. He was also a member of the Graduate Student Senate in 1969-70.

He was married to the former Patricia Joanne Brooks of Philadelphia, Pennsylvania on July 13, 1968. They have a daughter, Deidre Lynn, born on January 3, 1971.